The Plant Cell, Vol. 30: 907–924, April 2018, www.plantcell.org © 2018 ASPB.

Targeted Recruitment of the Basal Transcriptional Machinery by LNK Clock Components Controls the Circadian Rhythms of Nascent RNAs in Arabidopsis

Yuan Ma,[a] Sergio Gil,[a] Klaus D. Grasser,[b] and Paloma Mas[a,c,1]

[a] Centre for Research in Agricultural Genomics, CSIC-IRTA-UAB-UB, Campus UAB, Bellaterra, 08193 Barcelona, Spain
[b] Department of Cell Biology and Plant Biochemistry, Biochemistry Center, University of Regensburg, D-93053 Regensburg, Germany
[c] Consejo Superior de Investigaciones Científicas, 08028 Barcelona, Spain

ORCID IDs: 0000-0001-8975-1975 (Y.M.); 0000-0002-7080-5520 (K.D.G.); 0000-0002-3780-8041 (P.M.)

The rhythms of steady-state mRNA expression pervade nearly all circadian systems. However, the mechanisms behind the rhythmic transcriptional synthesis and its correlation with circadian expression remain fully unexplored, particularly in plants. Here, we discovered a multifunctional protein complex that orchestrates the rhythms of transcriptional activity in *Arabidopsis thaliana*. The expression of the circadian oscillator genes *TIMING OF CAB EXPRESSION1/PSEUDO-RESPONSE REGULATOR1* and *PSEUDO-RESPONSE REGULATOR5* initially relies on the modular function of the clock-related factor REVEILLE8: its MYB domain provides the DNA binding specificity, while its LCL domain recruits the clock components, NIGHT LIGHT-INDUCIBLE AND CLOCK-REGULATED proteins (LNKs), to target promoters. LNKs, in turn, specifically interact with RNA Polymerase II and the transcript elongation FACT complex to rhythmically co-occupy the target loci. The functional interaction of these components is central for chromatin status, transcript initiation, and elongation as well as for proper rhythms in nascent RNAs. Thus, our findings explain how genome readout of environmental information ultimately results in rhythmic changes of gene expression.

INTRODUCTION

Organisms have developed a complex mechanism that can anticipate the predictable changes in the surrounding environment to adjust their physiology and development in a timely manner (Zhang and Kay, 2010). This mechanism, known as the circadian clock, provides a remarkable adaptive advantage, allowing for the synchronization of internal biology with the external environment. In *Arabidopsis thaliana*, the clock machinery is quite sophisticated and involves reciprocal regulation among clock components that ultimately leads to biological rhythms that oscillate in resonance with the environment (Greenham and McClung, 2015). The organization of the circadian system in plants is hierarchical, with specific circadian coupling or communication among clock cells at the plant shoot apex that is important for clock synchronization in roots (Takahashi et al., 2015). The coupling of cells at the vasculature also plays a role in synchronizing neighboring mesophyll cells (Endo et al., 2014). Differences in coupling and/or circadian function in different parts of the plant were also reported in various studies (Thain et al., 2002; James et al., 2008; Yakir et al., 2011; Wenden et al., 2012; Bordage et al., 2016).

Transcriptional regulation is one of the many layers underlying the circadian function in plants. Therefore, it is not surprising to find, at the core of the plant clock, a high number of transcription factors including, among others, the MYB domain proteins (Carré and Kim, 2002). Single MYB domain transcription factors such as CCA1 (CIRCADIAN CLOCK ASSOCIATED1) and LHY (LATE ELONGATED HYPOCOTYL) operate very close to the Arabidopsis circadian oscillator and belong to a family of 11 members that share close sequence similarity within the MYB-like domain. Five of these single MYB factors (REVEILLE/LHY-CCA1-LIKE [RVE/LCL] proteins) were assigned to a family subgroup based on the presence of the so-called LCL domain (; Farinas and Mas, 2011), which is absent in other members of the single MYB family. Analyses of Arabidopsis plants misexpressing the RVEs have provided some clues about their role in circadian clock function. For instance, plants misexpressing RVE8/LCL5 display changes in phase, period, and amplitude of key oscillator genes (Farinas and Mas, 2011; Rawat et al., 2011; Hsu et al., 2013). Furthermore, the activation of the dusk-expressed gene *TOC1/PRR1* (*TIMING OF CAB EXPRESSION1/PSEUDO-RESPONSE REGULATOR1*) by RVE8 is antagonized by CCA1 and involves changes in the pattern of Histone 3 acetylation at the *TOC1* promoter (Farinas and Mas, 2011). Activation of *TOC1* and *PRR5* (another member of the TOC1/PRR1 family) occurs through direct binding of RVE8 to their promoters and requires interaction with two members of the NIGHT LIGHT-INDUCIBLE AND CLOCK-REGULATED (LNK) protein family, which together with RVEs form a transcriptional coactivator complex (Xie et al., 2014; Xing et al., 2015). In addition to altered gene expression, plants misexpressing RVE8 and/or LNKs show a variety of phenotypes affecting anthocyanin accumulation, plant growth, and photoperiodic regulation of flowering time (Farinas and Mas, 2011; Rawat et al., 2011; Pérez-García et al., 2015; Gray et al., 2017). Overall, LNKs connect circadian gene expression, growth, and development with

[1] Address correspondence to paloma.mas@cragenomica.es.
The author responsible for distribution of materials integral to the findings presented in this article in accordance with the policy described in the Instructions for Authors (www.plantcell.org) is: Paloma Mas (paloma.mas@cragenomica.es).
www.plantcell.org/cgi/doi/10.1105/tpc.18.00052

IN A NUTSHELL

Background: Circadian clocks are internal time-keeping mechanisms that help organisms adapt to the environmental changes that occur during the day and night cycle. In *Arabidopsis thaliana*, the circadian clock consists of multiple transcriptional regulatory feedback loops. The clock-associated components RVE8 and LNK were previously shown to interact directly to regulate rhythmic anthocyanin biosynthesis. Together, they also act as transcriptional activator and coactivator of the key core clock genes *PRR5* and *TOC1*.

Question: How are the circadian rhythms in *PRR5* and *TOC1* transcription generated, and what roles are played by RVE8 and LNKs?

Findings: Our studies identified a multifunctional protein complex in which each component exerts specific functions that contribute to the regulation of *PRR5* and *TOC1* transcription. The MYB domain of RVE8 provides the DNA binding specificity, while its LCL domain is responsible for the interaction with LNKs. LNKs in turn recruit RNA Polymerase II and the transcription elongation factor SSRP1 (STRUCTURE-SPECIFIC RECOGNITION PROTEIN1) to facilitate the initiation and elongation of clock transcripts. Mutation or inactivation of the protein complex components affects the expression of *PRR5* and *TOC1* nascent RNAs, delays the mRNA steady-state rising phase, and reduces the amplitude. We found that the rhythms in nascent RNA synthesis controlled by the protein complex determine the steady-state mRNA circadian oscillation.

Next steps: It has been reported that LNKs function as transcriptional repressors, so it would be interesting to investigate the molecular mechanisms underlying their repressing function and how they might act as both corepressors and coactivators.

seasonal changes in daylength and temperature (Rugnone et al., 2013; Mizuno et al., 2014; Xie et al., 2014).

Genome readout of environmental information ultimately results in controlled changes in gene expression exerted at its basis by the transcriptional machinery. Transcription of coding genes requires different phases, including initiation, elongation, and termination, followed by maturation and decay. Transcription initiation relies on the formation of the preinitiation complex (PIC), which includes the RNA Polymerase II (RNA Pol II) and a number of transcription factors and chromatin-related complexes that modulate RNA Pol II activity (Lee et al., 1999; Näär et al., 2001). Following PIC formation, the highly conserved heptapeptide repeats within the RNA Pol II C-terminal domain (CTD) (Allison et al., 1988; Nawrath et al., 1990) are susceptible of phosphorylation at specific residues, which facilitate the recruitment of particular protein complexes and the progression of initiation or elongation, depending on the position of the phosphorylated residue (Buratowski, 2009; Hajheidari et al., 2013). For instance, phosphorylation of Serine 5 (S5P) within the RNA Pol II CTD allows RNA Pol II to escape the PIC and initiate transcription (Komarnitsky et al., 2000). Thus, S5P is found at the promoters and 5′ ends of genes and is usually considered to be a marker of transcription initiation and early elongation. During the transition from initiation to elongation, decreased accumulation of S5P coincides with a progressive increase in Serine 2 phosphorylation (S2P) (Margaritis and Holstege, 2008), which aids in the recruitment of factors required for elongation (Hajheidari et al., 2013) followed by subsequent mRNA polyadenylation and termination at the 3′ ends of genes (McCracken et al., 1997; Birse et al., 1998).

Transcript elongation is also modulated by a number of transcript elongation factors, which associate with RNA Pol II and act as histone chaperones, modifying histones or RNA Pol II activity (Jonkers and Lis, 2015). In Arabidopsis, the histone chaperone FACT (FACILITATES CHROMATIN TRANSCRIPTION) complex is composed of SSRP1 (STRUCTURE-SPECIFIC RECOGNITION PROTEIN1) and SPT16 (SUPPRESSOR OF TY16) (Van Lijsebettens and Grasser, 2014). The FACT complex localizes throughout genomic regions of actively transcribed genes, and its binding correlates with gene transcription (Duroux et al., 2004). Notably, the FACT complex rhythmically binds to the promoter of *TOC1*, with a waveform paralleling *TOC1* mRNA oscillation (Perales and Más, 2007). Knockdown plants with decreased expression of *SSRP1* and *SPT16* show alterations in vegetative and reproductive development, while null *ssrp1* mutant plants are lethal (Lolas et al., 2010). Furthermore, together with other transcript elongation factors, the FACT complex copurifies with elongating RNA Pol II (Antosz et al., 2017), which suggests that the Arabidopsis FACT complex assists transcript elongation with a similar function to that described in yeast (Xin et al., 2009) and humans (Orphanides et al., 1998).

Here, we uncover the mechanisms controlling the dusk-phased rhythms in nascent RNAs and steady-state mature mRNAs in Arabidopsis. We provide evidence that LNKs act as molecular switches that recruit the transcriptional machinery for transcript initiation and elongation in a timely manner. Consistently, LNK function is essential for sustaining the rhythms in nascent RNAs. Binding to the circadian target gene promoters relies on the sequence-dependent specificity provided by the MYB domain of RVE8, while direct interaction of the LCL domain with LNKs conveys LNKs to the target promoters. Together, our study uncovers the role of clock components in regulating circadian transcription by directly recruiting the transcriptional machinery.

RESULTS

The MYB Domain of RVE8 Provides the DNA Binding Specificity to the *TOC1* and *PRR5* Promoters

To investigate the modular nature of RVE8 and the contribution of RVE8 domains to the overall function of the full-length protein

(RVE8-FL), we cloned a truncated version of RVE8 lacking the C-terminal LCL domain (Figure 1A). The construct, named ΔLCL, also contains GFP as a tag and is expressed under the control of the cauliflower mosaic virus 35S promoter. We produced Arabidopsis plants expressing the *TOC1* promoter fused to luciferase (*TOC1pro:LUC*) (Perales and Más, 2007) and examined promoter activity in wild-type and ΔLCL-overexpressing (ΔLCL-ox) lines under constant light (LL) conditions. Although the degree of overexpression was not very high (Supplemental Figure 1A), *TOC1pro:LUC* rhythms showed a delayed phase, a long period, and a slightly decreased amplitude in ΔLCL-ox compared with the wild type (Figures 1B and 1C). The decreased amplitude was also evident when rhythms were examined under light/dark cycles (12 h of light/12 h of dark [LD]) (Figures 1D and 1E; Supplemental Figure 1B). The circadian phenotypes of *TOC1pro:LUC* in ΔLCL-ox resembled those of *rve8* mutants (Supplemental Figures 1C and 1D), suggesting that ΔLCL-ox might interfere with RVE8 function. The similarities of ΔLCL-ox and *rve8* pervade other RVE8 targets, as *PRR5* expression also showed reduced amplitude under both LL (Figure 1F) and LD (Figure 1G) cycles, as assayed by RT-qPCR. Consistent with previous reports, our results revealed that, under constant red light conditions, RVE8-FL-ox showed significantly shorter hypocotyls while *rve8* mutant seedlings displayed longer hypocotyls compared with the wild type. The hypocotyls of ΔLCL-ox were also longer than those of the wild type (Supplemental Figure 1E).

Effector domains can modulate the transcriptional activity of DNA binding domains. As RVE8 regulates *TOC1* and *PRR5* expression through direct binding to their promoters, we examined the DNA binding capabilities of ΔLCL protein. Chromatin immunoprecipitation (ChIP) assays showed an evident enrichment of ΔLCL at both the *TOC1* and *PRR5* promoters (Figures 1H and 1I), suggesting that the MYB domain in ΔLCL retains the ability to bind to the target promoters despite the lack of the LCL domain. However, the observation that ΔLCL binding is not accompanied by the transcriptional activation of *TOC1* and *PRR5* suggests that ΔLCL might be competing with the endogenous RVE8 for promoter binding. Plants overexpressing ΔLCL in the *rve8* mutant background (ΔLCL-ox *rve8*) showed a clearly delayed phase of *TOC1pro:LUC* activity, along with a long period and decreased amplitude (Supplemental Figure 1F). Altogether, our results suggest that binding might be necessary but not sufficient for activation; thus, the LCL domain might play a prevalent role in the activating function of RVE8.

We also used confocal microscopy to compare RVE8-FL and ΔLCL distribution. Analysis of subcellular localization in hypocotyls and roots (Supplemental Figures 1G and 1I) revealed that RVE8-FL preferentially localized to the nucleus, although cytoplasmic strands with a reticulated pattern were also observed under confocal microscope settings of high gain. ΔLCL protein was also localized to the nucleus, with no evident sign of cytoplasmic strands under any gain conditions (Supplemental Figures 1H and 1J). The difference might be due to the absence of LCL or the reduced degree of overexpression in ΔLCL-ox. The nuclear localization of ΔLCL is consistent with the predicted bipartite nuclear localization signal (positions 103 to 125) (Supplemental Figure 1K) and with ΔLCL binding to nuclear DNA.

Overexpression of LCL-ox Exerts a Dominant-Negative Function in the Regulation of *TOC1* and *PRR5* Expression

The LCL domain amino acid sequence is highly conserved among a wide range of plant lineages (Supplemental Figures 2 and 3). Our results suggest that this domain might play an important role in RVE8 activity. To explore its function, we transformed the LCL domain fused to GFP under the control of the 35S promoter (Figure 2A) into *TOC1pro:LUC* plants to generate LCL-overexpressing lines (LCL-ox) (Supplemental Figure 4A). Bioluminescence analyses showed that the rhythmic oscillation of *TOC1pro:LUC* was clearly affected in LCL-ox plants, with a delayed phase and severely reduced amplitude under both LL and LD conditions (Figures 2B to 2E; Supplemental Figures 4C and 4D). The phenotypes were more severe than the ones observed in *rve8* mutants or in ΔLCL-ox plants (Figures 1B to 1E; Supplemental Figures 1B to 1D). *PRR5* expression was also severely disrupted in LCL-ox plants under LL and LD conditions (Figures 2F and 2G). Consistent with the severity of the gene expression phenotypes, LCL-ox hypocotyls were significantly longer than those of the wild type, ΔLCL-ox, and the *rve8* mutant, indicating that overexpression of LCL interferes with RVE8 function and results in enhanced plant hyposensitivity to red light (Figure 2H). Similarly, a clear delayed flowering time phenotype was observed in LCL-ox (Supplemental Figures 4E and 4F). Overexpression of LCL in the *rve8* mutant background (LCL-ox *rve8*) resulted in severe circadian phenotypes following the same trend to that of LCL-ox in the wild-type background (Supplemental Figures 4H and 4I). LCL-ox *rve8* hypocotyls were also significantly longer than those of the wild type (Supplemental Figure 4J). These results, together with the finding that LCL-ox phenotypes were more severe than those observed in *rve8*, suggest a possible dominant-negative role not only for RVE8 function but also for other members of the RVE family.

Our ChIP results showed the lack of enrichment of LCL on the *TOC1* and *PRR5* promoters in LCL-ox plants, which suggests that the LCL-ox dominant-negative function is not due to competition with the endogenous RVE8 for promoter binding. Analyses of the subcellular localization of LCL showed both nuclear and cytoplasmic accumulation (Supplemental Figure 4G). Altogether, our results show that the nucleus-localized LCL domain is not able to bind to the target gene promoters, but the circadian expression of these target genes is severely reduced in LCL-ox plants.

The RVE-LNK Tandem Regulates Both RNA Pol II and H3K4me3 Occupancy

To get further insights into the mechanisms of LCL function in the control of circadian gene expression, we performed a yeast two-hybrid screening with the LCL domain as bait. High-confidence-score (predicted biological score) analyses identified the members of the LNK protein family as proteins that interact with the LCL domain (Figure 3A). In vitro pull-down assays with *Escherichia coli* expressing the LCL domain fused to GST and LNK1 protein fused to MBP (Maltose Binding Protein) revealed a faint but reproducible coimmunoprecipitation (co-IP) of LNK1 with the LCL domain but not with GST-ΔLCL or with beads containing MBP-GFP (Figure

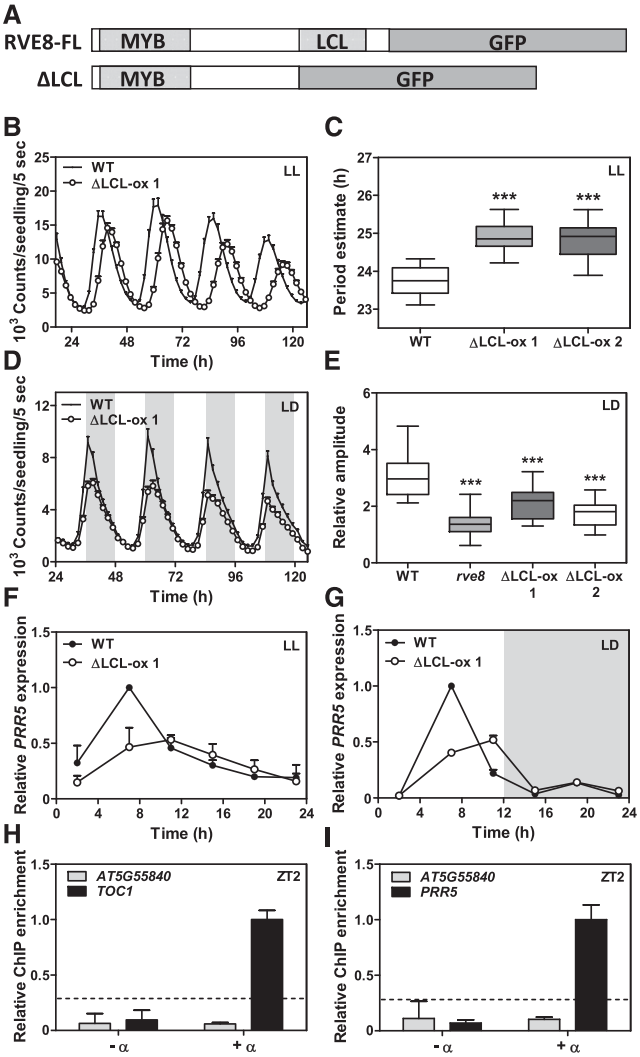

Figure 1. Overexpression of ΔLCL Alters *TOC1* and *PRR5* Circadian Gene Expression through the Binding of ΔLCL to Their Promoters.

(A) Schematic diagram depicting the full-length RVE8 protein (RVE8-FL) fused to GFP and a truncated version lacking the LCL domain (ΔLCL).

(B) Analysis of rhythmic oscillations of *TOC1pro:LUC* by in vivo luminescence assays in the wild type and ΔLCL-ox (line 1) under LL conditions.

(C) Period estimates of the circadian waveforms in the wild type and two different ΔLCL-ox lines (1 and 2) assayed as in **(B)** (***P < 0.001).

(D) Analysis of rhythmic oscillations of *TOC1pro:LUC* by in vivo luminescence assays in wild-type and ΔLCL-ox plants under LD cycles.

(E) Amplitude estimates of circadian waveforms in the wild type, *rve8* mutant, and two ΔLCL-ox lines assayed as in **(D)** (***P < 0.001).

(F) and **(G)** Time-course analysis by RT-qPCR assays of *PRR5* expression in wild-type and ΔLCL-ox plants grown under LL conditions for 2 d after synchronization under LD **(F)** or under LD cycles **(G)**. Data are represented as means + SE relative to *IPP2* (*ISOPENTENYL PYROPHOSPHATE:DIMETHYL-ALLYL PYROPHOSPHATE ISOMERASE*) expression and relative to the highest value.

(H) and **(I)** ChIP analyses with ΔLCL-ox plants assayed at ZT2 to examine binding to the *TOC1* **(H)** and *PRR5* **(I)** promoters. The promoter of the *AT5G55840* gene (*PPR*) was used as a negative control. Samples processed without (−α) and with (+α) antibody during the ChIP procedure are shown. ChIP enrichment is represented as means + SE relative to input and the highest value. Graphs include data from two biological replicates (samples from different starting material).

White and gray areas in **(D)** and **(G)** represent light and dark periods, respectively.

3B; Supplemental Figure 5A). An interaction was also observed for MBP-LNK3 with GST-LCL (Figure 3C; Supplemental Figure 5B). In vivo co-IP assays in plants using two different lines overexpressing both the LCL domain and LNK1 (LNK1-ox LCL-ox) revealed that the LCL domain effectively coimmunoprecipitated with LNK1 (Figures 3D and 3E). Co-IP was also observed in LNK3-ox LCL-ox plants (Figures 3F and 3G), which indicates the in vivo interaction of the LCL domain with LNK proteins.

As the rising phase of *TOC1* and *PRR5* expression is severely delayed in LCL-ox and in *lnk1 lnk2* double mutant plants, we hypothesized that the recruitment of the transcriptional machinery might be affected in these plants. Therefore, we assayed the distribution profiles of total RNA Pol II in wild-type and *lnk1 lnk2* plants. ChIP assays followed by qPCR showed that the accumulation of total RNA Pol II was reduced in *lnk1 lnk2* plants at the 5′ end, middle, and 3′ end regions of the *PRR5* and *TOC1* loci (Figures 4A to 4D; Supplemental Figures 5E and 5F). As RVE8 and RVE4 interact with LNKs (Xie et al., 2014), we also examined the enrichment of total RNA Pol II in *rve4 rve6 rve8* triple mutant plants. Our results showed a decreased enrichment of RNA Pol II in *rve4 rve6 rve8* compared with the wild type (Supplemental Figures 5C and 5D), suggesting that RNA Pol II binding at the *TOC1* and *PRR5* loci is altered in the absence of functional RVEs or LNKs. Analyses of the two main CTD-phosphorylated isoforms characteristic of transcription initiation (S5P) and elongation (S2P) showed that the enrichment of both was clearly reduced in *PRR5* and *TOC1*, most strikingly at Zeitgeber Time 7 (ZT7) and ZT11 (ZT0 is defined as the time of lights on) (Figures 4E to 4H), which coincide with their peak of expression and the time of RVE8 interaction with LNKs (Xie et al., 2014; Pérez-García et al., 2015). While, in wild-type plants, the RNA Pol II phosphorylated profiles clearly oscillated closely following the rhythms of gene expression, the oscillation was abolished in *lnk1 lnk2* plants (Figures 4E to 4H). These results suggest that LNK1 and LNK2 might be important for the circadian accumulation of RNA Pol II S5P and S2P at the *PRR5* and *TOC1* loci.

Different chromatin marks correlate with the occupancy of the transcriptional machinery. As this occupancy is altered in *lnk1 lnk2* plants, we asked whether chromatin marks were also affected. To this end, we examined the accumulation of trimethylated lysine 4 of Histone 3 (H3K4me3), a mark generally associated with transcriptionally active genes (Shukla et al., 2009). H3K4me3 accumulation is also important for a precise circadian oscillation and proper amplitude of clock gene expression (Malapeira et al., 2012). Our ChIP data showed that H3K4me3 accumulation was clearly reduced in *lnk1 lnk2* plants, primarily at ZT7 and ZT11, while no appreciable differences were observed at ZT3 (Figures 4I and 4J). Altogether, our results suggest that alteration of chromatin status as well as transcriptional initiation and elongation correlate with the altered waveforms of circadian gene expression in *lnk1 lnk2* plants.

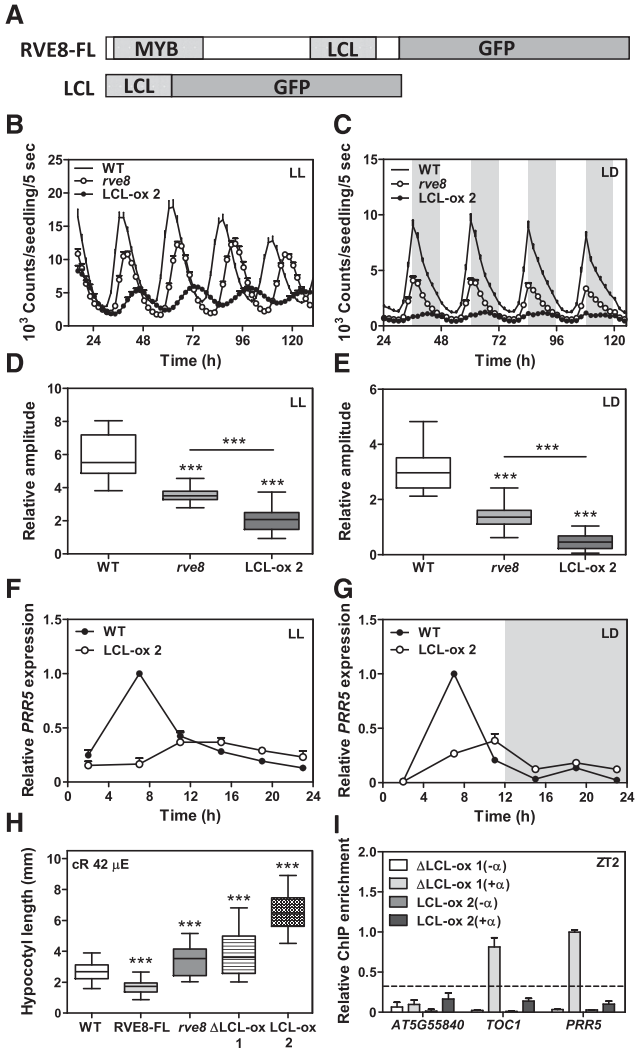

Figure 2. Alteration of Circadian Gene Expression and Hypocotyl Elongation in LCL-ox Plants.

(A) Schematic diagram depicting RVE8-FL fused to GFP and a truncated version consisting of the LCL domain.

(B) Analysis of rhythmic oscillations of *TOC1pro:LUC* by in vivo luminescence assays in the wild type, *rve8* mutant, and LCL-ox (line 2) grown under LL conditions following synchronization under LD cycles.

(C) Analysis of rhythmic oscillations of *TOC1pro:LUC* by in vivo luminescence assays in wild-type, *rve8* mutant, and LCL-ox plants under LD cycles.

(D) and **(E)** Amplitude estimates of circadian waveforms in wild-type, *rve8* mutant, and LCL-ox plants assayed as in **(B)** and **(C)**, respectively (***P < 0.001).

(F) and **(G)** Time-course analysis by RT-qPCR assays of *PRR5* expression in wild-type and LCL-ox plants grown under LL cycles **(F)** or under LD conditions **(G)**. Data are represented as means + SE of two biological replicates (samples from different starting material) relative to *IPP2* expression and the highest value.

(H) Hypocotyl length of the wild type, RVE8-FL-ox, *rve8*, ΔLCL-ox, and LCL-ox lines grown under constant red light (42 μmol·quanta·m^{-2}·s^{-1} [μE]). Data are means ± SE of two biological replicates (samples from different starting material) (***P < 0.001).

LNKs Directly Interact with RNA Pol II and the FACT Complex

The severely reduced clock gene expression and reduced accumulation of RNA Pol II at the clock gene loci in *lnk1 lnk2* plants suggest a possible role for LNKs in recruiting the transcriptional machinery. To explore this possibility, we first checked the direct interaction of LNKs with RNA Pol II by in vitro pull-down studies using the CTD fused to GST and LNK1 fused to MBP. Our results showed efficient immunoprecipitation of GST-CTD (Supplemental Figure 6A) and reproducible MBP-LNK1 copurification with GST-CTD, whereas no interaction was observed with GST alone used as a negative control (Supplemental Figure 6B). The interaction was then assayed with protein extracts from LNK1-ox plants incubated with an anti-MYC antibody to immunoprecipitate LNK1. The immunoprecipitated protein complexes were then analyzed for total RNA Pol II. The antibody recognized phosphorylated and nonphosphorylated isoforms (Figure 5A, upper panel). Although we observed slightly higher accumulation of the nonphosphorylated protein (Figure 5A, upper panel), the phosphorylated isoforms were effectively immunoprecipitated with LNK1 (Figure 5B, upper panel). These results were confirmed in co-IP studies with specific antibodies recognizing CTD S5P and CTD S2P. Although a weak signal background was observed in wild-type plants and both antibodies had some cross-reactivity with nonphosphorylated isoforms, our results showed that S5P and S2P reproducibly coimmunoprecipitated with LNK1 (Figure 5B, middle and lower panels). Thus, LNK1 functions as a transcriptional coactivator that directly interacts with RNA Pol II. The interaction with S5P and S2P RNA Pol II isoforms also suggests that LNK1 might engage in the regulation of transcript initiation and elongation.

Our previous studies have shown that not only chromatin marks but also the binding of the histone chaperone complex FACT rhythmically oscillates at the *TOC1* promoter (Perales and Más, 2007). Furthermore, FACT forms part of a transcription elongation complex containing RNA Pol II (Antosz et al., 2017). To examine whether LNKs are also part of this complex, we performed in vitro pull-down studies of LNKs and SSRP1, a component of the FACT complex. Our results showed that both MBP-LNK1 (Figure 5C) and MBP-LNK3 (Figure 5D) coimmunoprecipitated with GST-SSRP1. To assay the interaction in vivo, protein extracts from plants overexpressing either LNK1 or LNK3 were immunoprecipitated with an anti-MYC antibody and analyzed with an anti-SSRP1 antibody (Duroux et al., 2004; Antosz et al., 2017). Although the amount of detected LNK1 protein was very low due to technical issues (Figure 5E), SSRP1 was still efficiently coimmunoprecipitated (Figure 5F). The use of LNK3-ox plants revealed that SSRP1 also interacted with LNK3 (Figures 5E and 5F). Altogether,

(I) ChIP analyses of ΔLCL-ox and LCL-ox plants assayed at ZT2 to examine the binding of ΔLCL and LCL, respectively, to the *TOC1* and *PRR5* promoters. The promoter of the *AT5G55840* gene (*PPR*) was used as a negative control. Samples processed without (−α) and with (+α) antibody during the ChIP procedure are shown. ChIP abundance is represented as means + SE of two biological replicates (samples from different starting material) and relative to the highest value.

White and gray areas in **(C)** and **(G)** represent light and dark periods, respectively.

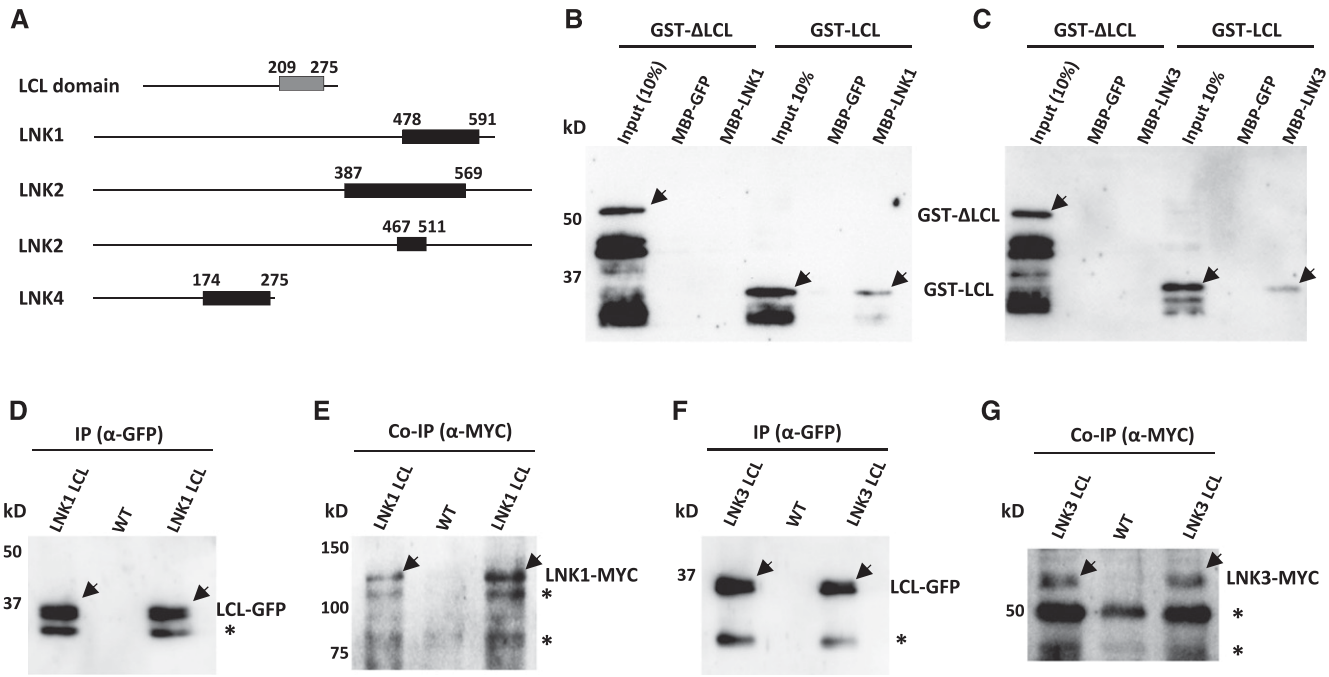

Figure 3. Direct Interaction of LNKs with the LCL Domain of RVE8.

(A) The coding sequence of the LCL domain (nucleotides 627 to 825, amino acids 209 to 275; gray box) was used as a bait in a yeast-two hybrid screen with a random-primed cDNA library from Arabidopsis. Selected interaction domains (black boxes) from LNKs were obtained by identifying the domains shared by all prey fragments matching the reference protein.

(B) and **(C)** In vitro pull-down assays of ΔLCL and LCL with LNK1 **(B)** and LNK3 **(C)**. Protein complexes were purified using amylose resin to detect GST fusion proteins (GST-ΔLCL and GST-LCL).

(D) to **(G)** Immunoblot analysis of two different double overexpressing LNK1-MYC-ox LCL-YFP-ox lines (**[D]** and **[E]**) and LNK3-MYC-ox LCL-YFP-ox (**[F]** and **[G]**). Protein extracts were immunoprecipitated (IP) with anti-GFP antibody (**[D]** and **[F]**) following detection with anti-MYC antibody (co-IP) (**[E]** and **[G]**). Wild-type protein extracts were similarly processed. Plants were grown under LD cycles for 10 d and processed at ZT7. Arrows indicate the specific detected proteins, while asterisks indicate unspecific or degraded protein products.

these results indicate that LNKs, RNA Pol II, and SSRP1 form part of the same protein complex.

If LNKs interact with RNA Pol II and the FACT complex, functional LNKs should localize to the *PRR5* and *TOC1* loci. Indeed, ChIP assays using LNK1-ox plants showed significant enrichment of LNK1 binding to *PRR5* and *TOC1* (Supplemental Figures 6C and 6D) compared with unrelated loci or with samples similarly processed but excluding incubation with the antibody (-α) (Supplemental Figures 6C and 6D). Although the size of sonicated chromatin required for efficient ChIP assays precludes obtaining a very precise spatial resolution, qPCR amplification at the 5′, middle, or 3′ region of *PRR5* and *TOC1* loci confirmed a significant enrichment at the 5′ ends of the genes, although above background amplification was also observed in the middle and 3′ ends of the genes (Supplemental Figures 6C and 6D). Notably, when the same distribution analyses were performed for RVE8, we found enrichment only at the 5′ end of the *PRR5* and *TOC1* genes (Supplemental Figures 6E and 6F). These results suggest that RVE8 recruits LNKs to the *PRR5* and *TOC1* promoters but that LNKs, together with RNA Pol II and the FACT complex, travel along the *PRR5* and *TOC1* loci. These results are also consistent with a role for LNKs in the regulation of *PRR5* and *TOC1* transcript initiation and elongation.

LNKs and the FACT Complex Co-Bind to *PRR5* and *TOC1* Loci and Regulate Their Circadian Transcription

Our results suggest that LNKs might aid in recruiting the transcriptional machinery to the target genes *PRR5* and *TOC1*. To investigate this hypothesis, we examined the occupancy of SSRP1 at the *PRR5* and *TOC1* loci via ChIP assays. In wild-type plants, SSRP1 was detected at *PRR5* and *TOC1*, whereas reduced accumulation was observed at the transcriptionally inactive retrotransposon TA3 (Figure 6A). In *lnk1 lnk2* plants, we found reduced SSRP1 occupancy close to background levels (Figure 6A), which suggests that LNKs might be important for proper SSRP1 association to the *PRR5* and *TOC1* loci. These results are consistent with the reduced S2P occupancy in *lnk1 lnk2* plants, which was specific for *PRR5* and *TOC1* loci but not for *ACT7* (*ACTIN7*) (Supplemental Figure 7A).

If LNKs form part of the same protein complex as FACT and RNA Pol II, then the lack of a functional FACT complex should affect RNA Pol II, which transits from the PIC to the initiation phase. This would lead to the failure of RNA Pol II to engage in the elongation phase, since an efficient passage through nucleosomal structures cannot be supported by a compromised FACT complex. Thus, we assayed the occupancy of RNA Pol II CTD-phosphorylated isoforms in *ssrp1* mutant plants. As SSRP1 is critical for viability

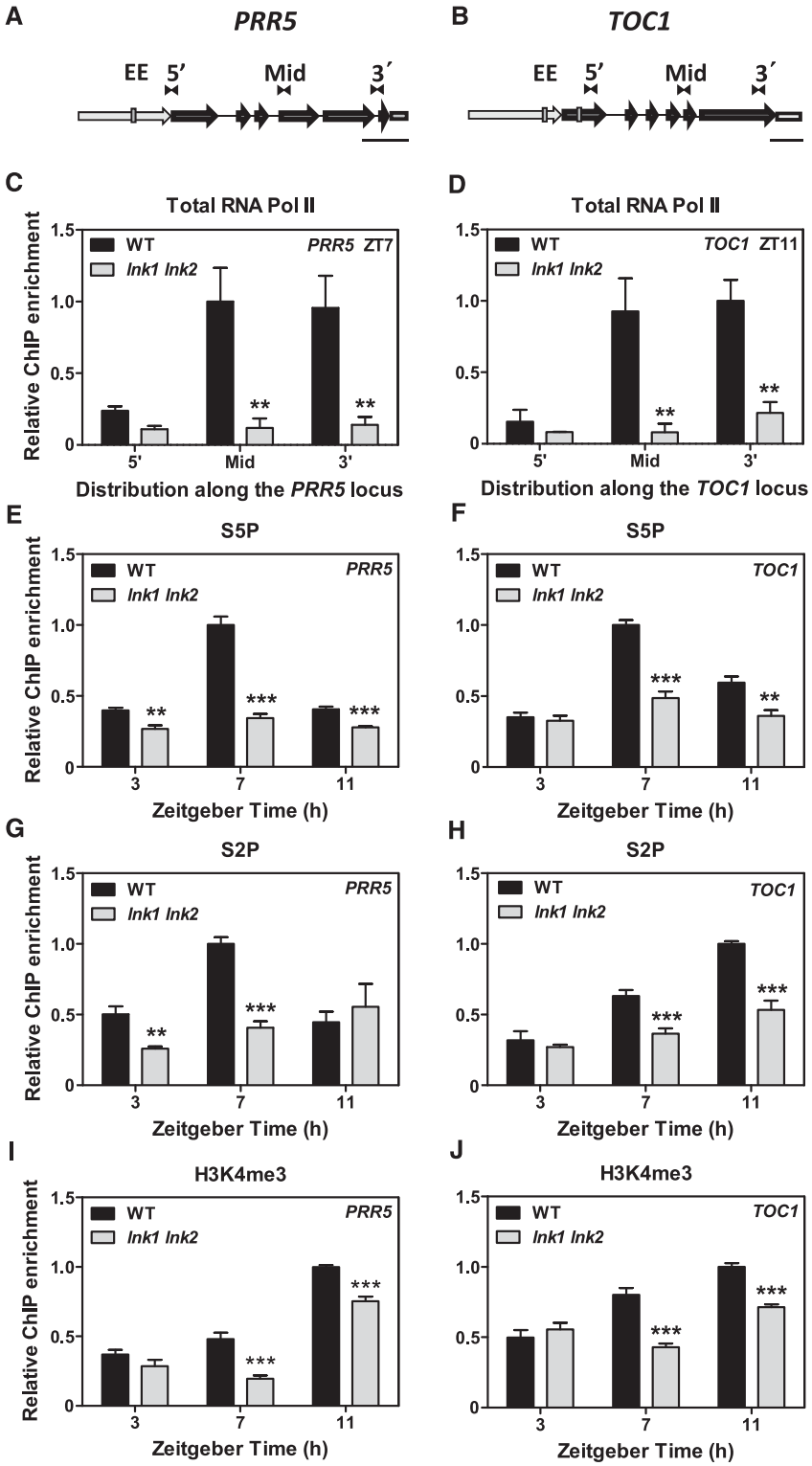

Figure 4. RNA Pol II and H3K4me3 Deposition at the *PRR5* and *TOC1* Loci Are Altered in *lnk1 lnk2* Double Mutant Plants.

(A) and **(B)** Diagrams depicting *PRR5* **(A)** and *TOC1* **(B)** loci. Double arrowheads indicate the primer positions for amplification of the 5′ end, middle (Mid), and 3′ end regions of each locus. Gray boxes represent evening element (EE) positions. Bars = 500 bp.

(Duroux et al., 2004), we used *ssrp1-2* mutant plants with a 50% reduction in *SSRP1* transcript accumulation (Lolas et al., 2010). We found that the accumulation of both phosphorylated isoforms was reduced at the *PRR5* and *TOC1* loci (Figures 6B and 6C; Supplemental Figures 7B and 7C). When we compared S2P occupancy in wild-type, *lnk1 lnk2*, and *ssrp1-2* plants, we found a similar marked reduction in S2P accumulation in *lnk1 lnk2* and *ssrp1-2* at *PRR5* and *TOC1* but not at *ACT7* (Supplemental Figure 7D). The reduction in RNA Pol II accumulation in *ssrp1-2* mutant plants was accompanied by a delayed rising phase and a marked decrease in *PRR5* expression at ZT7 (Figure 6D). Although *ssrp1-2* plants are only knockdown mutants, the circadian phenotypes of gene expression closely resembled those observed in ΔLCL-ox and LCL-ox (Figures 6E and 6F). Consistently, RNA Pol II S5P and S2P accumulation was also significantly reduced in ΔLCL-ox and LCL-ox plants (Supplemental Figures 7E and 7F). These results, together with the direct protein-protein interaction data, support the idea that LNKs and the FACT complex contribute together to the regulation of *PRR5* and *TOC1* circadian transcription.

To further support the functional relevance of LNKs and the FACT complex, we performed sequential ChIP assays to identify the possible co-binding of LNK1 and the FACT complex at the clock loci. Control analyses of double anti-MYC immunoprecipitation rounds in LNK1-ox plants revealed the enrichment of LNK1 at the *TOC1* promoter and verified the reliability of the double round of immunoprecipitation (Figure 6G). Immunoprecipitation with the anti-MYC antibody to pull down LNK1 followed by a second round of immunoprecipitation with the anti-SSRP1 antibody revealed that both proteins form part of the same complex, which binds to the middle and 3′ end regions of the *TOC1* locus (Figure 6H).

The interaction of LNKs with the elongating S2P CTD RNA Pol II and with SSRP1, together with its distribution along the target genes, suggests a role for LNKs in both transcript initiation and elongation. If that is the case, the pharmacological inhibition of transcript initiation and elongation should resemble the *lnk1 lnk2* phenotypes. To examine this possibility, we performed bioluminescence analyses with plants treated with kinase inhibitors such as flavopiridol (Flap) and seliciclib (Selic), which inhibit the CTD phosphorylation of S5 and S2, respectively (Ding et al., 2011). Our results showed a dose-dependent decreased amplitude and delayed phase of *TOC1pro:LUC* activity (Figures 7A to 7C; Supplemental Figures 8A to 8C), which indeed resembled the phenotypes of *lnk1 lnk2* plants. These results are consistent with the decreased binding of RNA Pol II (S5P and S2P) and SSRP1 to the *PRR5* and *TOC1* loci in plants treated with the inhibitors (Supplemental Figures 8G to 8I). We also reasoned that if the recruitment of the machinery responsible for clock transcript initiation and elongation is affected in *lnk1 lnk2* plants, then the effect of these inhibitors should be diminished in *lnk1 lnk2* compared with wild-type plants. Indeed, RT-qPCR analyses showed a delayed phase and evident reduction of *PRR5* and *TOC1* amplitude in inhibitor-treated wild-type plants (Figure 7D; Supplemental Figure 8D), while only a minor effect was observed in *lnk1 lnk2* plants (Figures 7E and 7F) and in the *rve4 rve6 rve8* triple mutant (Supplemental Figures 8E and 8F). Therefore, treatment of *lnk1 lnk2* plants with inhibitors had only a minor impact, as S5P and S2P accumulation is already affected in these plants. In agreement with our conclusions, the interaction of LNKs with SSRP1 was reduced following treatment with Selic, while SSRP1, LNK1, and LNK3 protein accumulation was not significantly affected by the treatment (Supplemental Figures 8J to 8M). Taken together, our results indicate that the function of LNKs is important for transcript initiation and the elongation of *PRR5* and *TOC1*.

The Rhythms of *PRR5* and *TOC1* Nascent RNAs Are Affected in *lnk1 lnk2* Plants

Our results suggest that LNKs affect *PRR5* and *TOC1* transcription, but their effects on gene expression were analyzed using steady-state mRNA. Therefore, we examined actual changes in transcript synthesis by analyzing nascent RNAs in wild-type and *lnk1 lnk2* plants. To this end, we isolated nuclei from plants sampled at ZT3, ZT7, and ZT11 and performed nuclear run-on transcription by bromouridine immunocapture, followed by the detection of labeled nascent transcripts by RT-qPCR. The primers used for nascent RNA detection (nr1, nr3, and nr5) spanned exon-intron boundaries (to exclude the amplification of possible mature spliced mRNA) along the 5′ end, gene body, and 3′ end of the genes (Supplemental Figure 9). In wild-type plants, *PRR5* and *TOC1* nascent RNAs exhibited a 5′ to 3′ gradient at each time point (Figures 7G to 7L). In addition, the peak accumulation of nascent RNAs correlated with the peak of steady-state mRNAs (i.e., ZT7 for *PRR5* and ZT11 for *TOC1*) (Figures 7G to 7L; Supplemental Figures 9C and 9D). The use of primers spanning two exons (ex-ex) rendered very low amplification, indicating the lack of mature mRNA contamination (Figures 7H and 7L). In *lnk1 lnk2* plants, nascent RNA accumulation was significantly low at all time points examined (Figures 7G to 7L; Supplemental Figures 9C and 9D). Reduced

Figure 4. (continued).

(C) and **(D)** ChIP-qPCR analyses of total RNA Pol II enrichment at the 5′ end, middle, and 3′ end regions of *PRR5* **(C)** and *TOC1* **(D)** in wild-type and *lnk1 lnk2* plants assayed at ZT7 and ZT11, respectively.

(E) and **(F)** ChIP-qPCR analyses of CTD S5P enrichment at the 5′ terminus in *PRR5* **(E)** and *TOC1* **(F)** in wild-type and *lnk1 lnk2* plants assayed at ZT3, ZT7, and ZT11.

(G) and **(H)** ChIP-qPCR analyses of CTD S2P enrichment at the middle regions in *PRR5* **(G)** and *TOC1* **(H)** in wild-type and *lnk1 lnk2* plants assayed at ZT3, ZT7, and ZT11.

(I) and **(J)** ChIP-qPCR enrichment of H3K4me3 in *PRR5* **(I)** and *TOC1* **(J)** in wild-type and *lnk1 lnk2* plants assayed at ZT3, ZT7, and ZT11 at the 5′ terminus. Data are represented as means + SE and relative to *ACTIN7* (*ACT7*) and the highest value. Graphs include data from two biological replicates (samples from different starting material). $^{**}P < 0.01$ and $^{***}P < 0.001$.

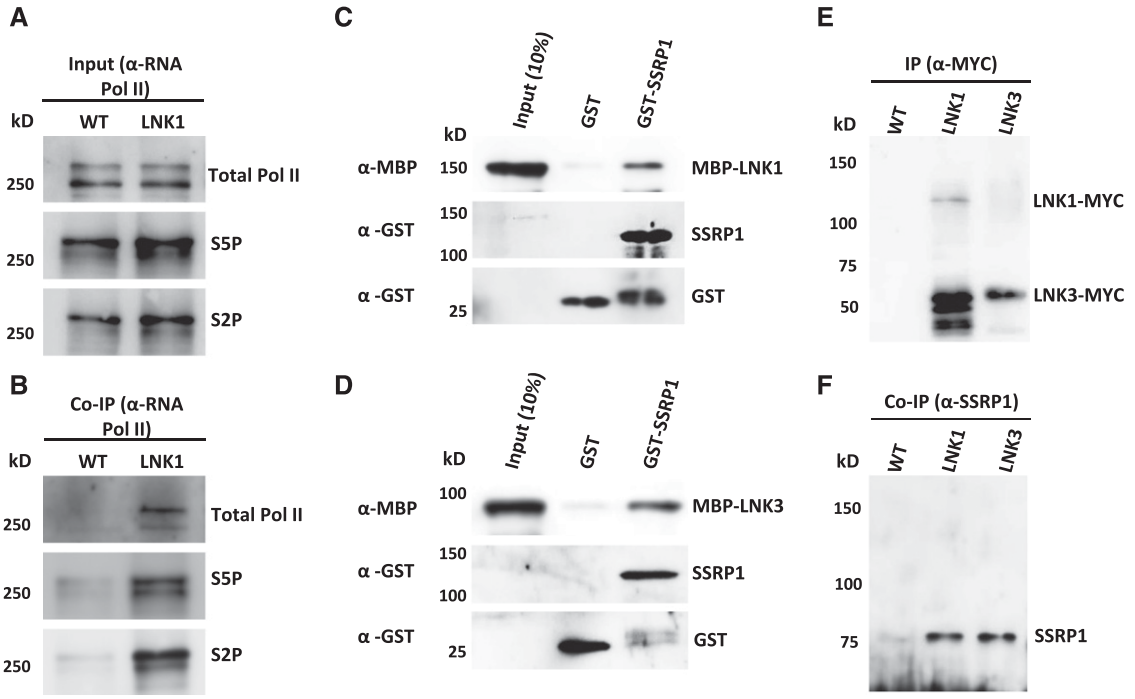

Figure 5. Direct Interaction of LNKs with the RNA Pol II and the Component of the FACT Complex SSRP1.

(A) and **(B)** Input of total RNA Pol II and the phosphorylated isoforms S5P and S2P **(A)** and co-IP with anti-MYC antibody following detection with anti-total RNA Pol II, S5P, and S2P antibodies **(B)** in wild-type and LNK1-ox plants.

(C) and **(D)** In vitro pull-down assays of SSRP1 with LNK1 **(C)** and LNK3 **(D)**. Protein complexes were purified using Glutathione Sepharose resin to detect MBP-fused proteins (MBP-LNK1 and MBP-LNK3).

(E) and **(F)** Co-IP assays by protein gel blot analysis of LNK1-MYC-ox and LNK3-MYC-ox.Plant protein extracts were immunoprecipitated with anti-MYC antibody following detection with anti-MYC antibody (IP) and anti-SSRP1 antibody (co-IP).

Plants were grown under LD cycles for 10 d and processed at ZT7.

nascent RNA accumulation in *lnk1 lnk2* plants was observed at the 5′ ends and at the gene bodies, suggesting that both transcript initiation and elongation were affected (changes in elongation would result in differences in the gene body but not at the 5′ terminus). The effect was specific to *PRR5* and *TOC1*, as nascent RNAs of a control gene such as *UBQ5* (UBIQUITIN5) showed similar accumulation patterns in wild-type and *lnk1 lnk2* plants (Figures 7H, 7I, 7K, and 7L). Together, these results indicate that, not only are the steady-state levels of *PRR5* and *TOC1* mRNA rhythmically expressed, but their nascent RNAs are as well. Our results also demonstrate that LNKs are important for the accumulation of these nascent RNAs.

Altogether, our results identify a multifunctional protein complex in which each component exerts specific functions in a timely manner that ultimately contribute to the temporal control of transcriptional synthesis of the clock genes *PRR5* and *TOC1* (Supplemental Figure 9E). The MYB domain of RVE8 provides DNA binding specificity, while its LCL domain is responsible for the interaction with LNKs. LNKs, in turn, recruit RNA Pol II and SSRP1 to facilitate the initiation and elongation of clock transcripts. The functions of all these components are essential, as mutation or inactivation of these activities affects nascent RNAs, delays the mRNA steady-state rising phase, and reduces the amplitude of the clock genes *PRR5* and *TOC1*.

DISCUSSION

Most transcription factors are modular, with DNA binding and effector domains that are responsible for the regulation of transcriptional activity (Du et al., 2009). Here, we functionally mapped the different RVE8 domains and found that the MYB domain is sufficient for DNA binding to target genes, while the LCL domain is responsible for the interaction with LNKs. The MYB family represents a large class of proteins that generally function as transcription factors (Dubos et al., 2010). Most of these proteins contain several imperfect repeats of a highly conserved MYB domain at their N termini. A particular subclass of MYB proteins has been separately grouped based on the presence of a single or partial MYB repeat. Based on structural properties, it is likely that the single MYB domain binds DNA in a different way from proteins containing several MYB repeats (Jin and Martin, 1999). Some members of the single MYB protein family have been characterized in several plant species and were shown to be involved in the regulation of secondary metabolism, cellular and organ morphogenesis, as well as circadian rhythms (Carré and Kim, 2002).

Unlike the highly conserved MYB domain at the N terminus, the C-terminal end is usually variable and is responsible for modulating the transcriptional activity of the protein. The LCL domain is

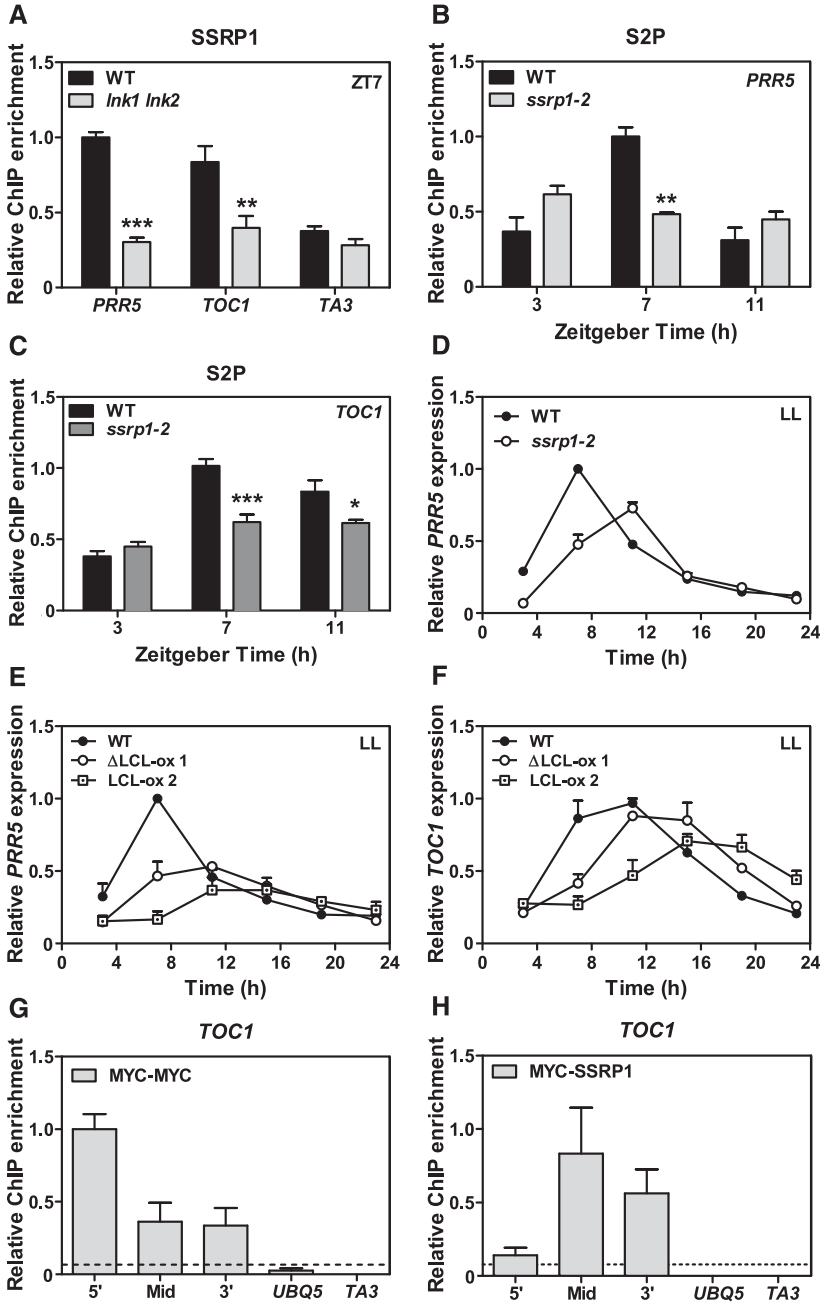

Figure 6. The Coordinated Function of SSRP1 and LNKs Is Important for RNA Pol II Recruitment and Circadian Gene Expression of Core Clock Genes.

(A) SSRP1 occupancy at the *PRR5*, *TOC1*, and *TA3* loci by ChIP assays in wild-type and *lnk1 lnk2* plants.

(B) and **(C)** Time-course analyses of CTD S2P profiles in *PRR5* **(B)** and *TOC1* **(C)** in the wild type and *ssrp1-2* at ZT3, ZT7, and ZT11.

(D) to **(F)** Time-course analysis by RT-qPCR of *PRR5* expression (**[D]** and **[E]**) and *TOC1* **(F)** in wild-type and *ssrp1-2* plants **(D)** and in wild-type, ΔLCL-ox, and LCL-ox plants (**[E]** and **[F]**) under LL conditions for 2 d after synchronization under LD. Data are represented as means + SE relative to *IPP2* expression and to the highest value.

(G) and **(H)** ChIP enrichment after a double round of immunoprecipitation with anti-MYC and anti-MYC antibodies **(G)** and with anti-MYC and anti-SSRP1 antibodies **(H)** to detect colocalization of LNK1 and SSRP1 at the *TOC1* gene body. ChIP enrichment is represented as means + SE relative to the input and to the highest value. *UBIQUITIN5* (*UBQ5*) and *TA3* were used as negative controls.

Data are represented as means + SE of two biological replicates (samples from different starting material). *P < 0.05, **P < 0.01, and ***P < 0.001.

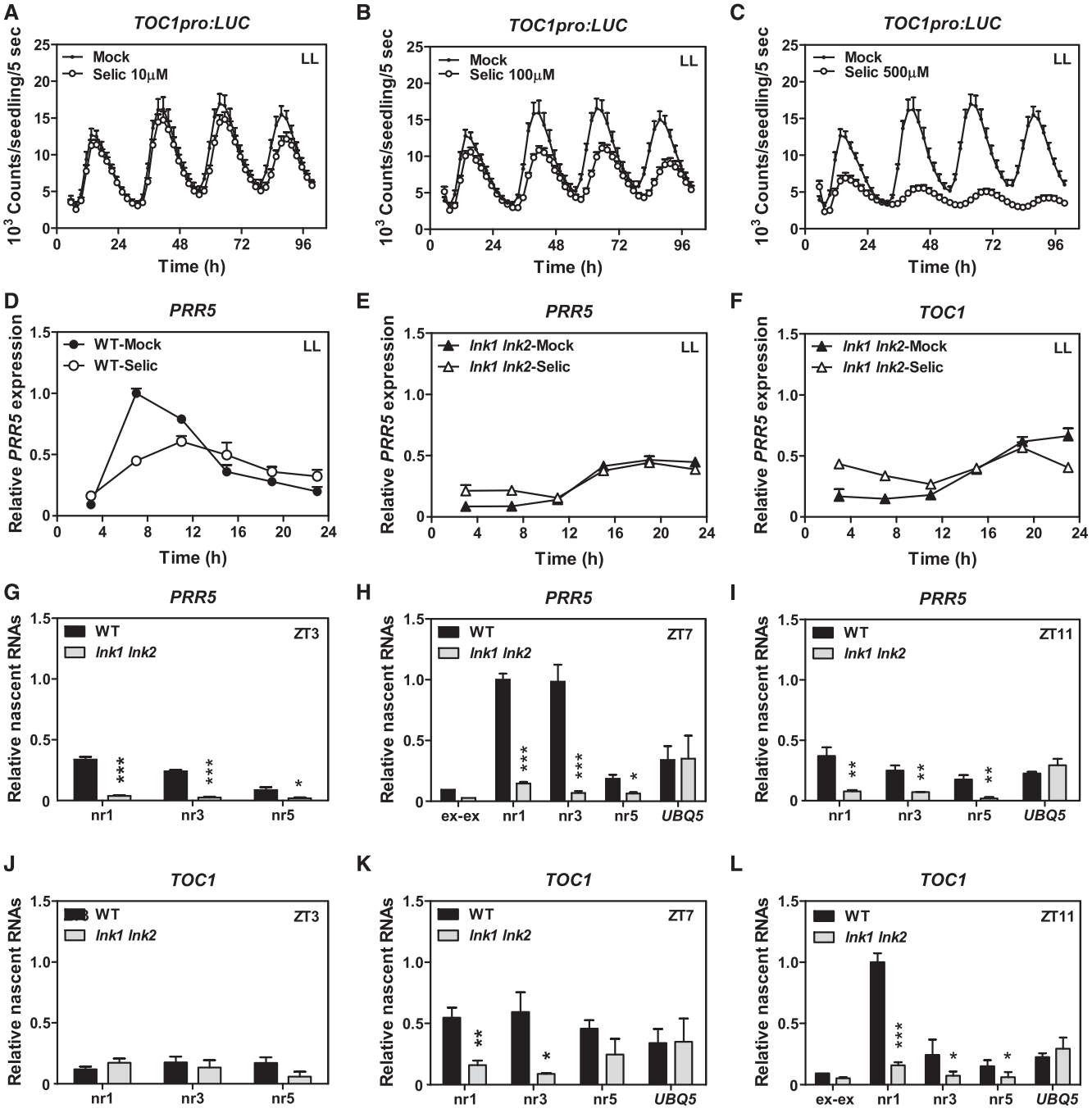

Figure 7. Role of LNKs in the Regulation of *PRR5* and *TOC1* Transcript Synthesis.

(A) to **(C)** Analysis of rhythmic oscillations of *TOC1pro:LUC* by in vivo luminescence assays in wild-type plants grown under LL conditions following synchronization under LD cycles treated with the indicated concentrations of seliciclib (Selic). Data are represented as means + SE of two biological replicates (samples from different starting material).

(D) to **(F)** Time-course analysis by RT-qPCR of *PRR5* (**[D]** and **[E]**) and *TOC1* **(F)** expression in wild-type **(D)** and *lnk1 lnk2* (**[E]** and **[F]**) plants in the absence or presence of Selic. Analyses were performed under LL conditions for 2 d after synchronization under LD. Data are represented as means + SE relative to *18S rRNA* expression and to the highest value.

(G) to **(L)** *PRR5* (**[G]** to **[I]**) and *TOC1* (**[J]** to **[L]**) nascent RNA accumulation at ZT3 (**[G]** and **[J]**), ZT7 (**[H]** and **[K]**), and ZT11 (**[I]** and **[L]**) using different sets of exon-intron primers along the loci (nr, nascent RNA primers). Nascent RNAs of *UBQ5* were also analyzed as a control (**[H]**, **[I]**, **[K]**, and **[L]**). Data are represented as means + SE relative to *ACT7* and to the highest value.

Graphs include data from two biological replicates (samples from different starting material). *P < 0.05, **P < 0.01, and ***P < 0.001.

exclusively found in the five members of the RVE/LCL subclass and is responsible for the interaction with LNKs. The binding and cooperative action of MYB proteins with other transcription factors are important for the control of numerous processes, including flavonoid biosynthesis, drought responses, epidermal differentiation, and patterning in root hairs and trichomes (Du et al., 2009). We found that the interaction of the RVE8 LCL domain with LNKs is central for controlling the circadian expression of core clock components such as *PRR5* and *TOC1*. Previous studies have already shown that RVEs and LNKs are cotranscriptional activators of circadian gene expression (Xie et al., 2014) but display an antagonistic function in the control of anthocyanin gene expression (Pérez-García et al., 2015).

Our understanding of the components and mechanisms of transcription in plants has been lagging behind that of animal systems. Global nuclear run-on sequencing and RNA sequencing have recently shown that, in plants, nascent transcripts correlate with steady-state transcript accumulation (Hetzel et al., 2016). This study also revealed the lack of divergent transcription or promoter-proximal pausing in plants, which are commonly found in other species (Preker et al., 2008; Jonkers and Lis, 2015). These results suggest that initiation is an important regulatory step in transcription in plants (Hetzel et al., 2016). Studies performed with a biochemically inactive variant of the SET-related protein ARABIDOPSIS HOMOLOG OF TRITHORAX1 (ATX1) revealed that promoter-proximal pausing can indeed be observed in plants (Ding et al., 2012). Further support of this notion was provided by another study showing cooperativity between SQUAMOSA PROMOTER BINDING PROTEIN-LIKE15 and SUPPRESSOR OF OVEREXPRESSION OF CONSTANS1 for the activation of *FRUITFULL* (Hyun et al., 2016).

Studies performed in *Drosophila melanogaster* (Rodriguez et al., 2013) and mouse (Menet et al., 2012) have shown that posttranscriptional regulation plays a crucial role in the regulation of circadian mRNA expression. Our results show that the expression of *PRR5* and *TOC1* nascent RNAs is rhythmic and follows the same oscillatory trend as steady-state mature mRNA. The rhythms were disrupted and the amount of nascent RNAs significantly reduced in *lnk1 lnk2* plants, which suggest that LNKs are important for proper rhythmic accumulation of *PRR5* and *TOC1* nascent RNAs. Our results show that LNKs bind to the 5′ regions of the *PRR5* and *TOC1* loci. LNKs interact with RNA Pol II S5P, and proper accumulation of RNA Pol II S5P also requires functional LNKs. Together with the repressed and delayed transcription of *PRR5* and *TOC1* in *lnk1 lnk2* plants, respectively, we conclude that LNKs are important for transcriptional initiation of *PRR5* and *TOC1*. LNKs aid in the recruitment of the transcriptional machinery to circadian targets. Target specificity is provided by the sequence-dependent binding of RVE8 to the *PRR5* and *TOC1* loci. The subsequent recruitment of RNA Pol II thus ensures proper circadian timing for the transcriptional machinery.

Our results also suggest that transcriptional elongation is modulated by RVE8 and LNKs. Two distinctive processes delineate transcriptional elongation: processivity (nucleotide additions per initiation event) and the elongation rate (nucleotide additions/min) (Mason and Struhl, 2005). Both a reduced and slow elongation rate of RNAP II might lead to premature dissociation along the chromatin template (Mason and Struhl, 2005). Our results show that LNKs interact with RNA Pol II S2P and with the elongation factor SSRP1 such that the observed reduced occupancy in the *lnk1 lnk2* double mutant might be due to their improper recruitment, leading to altered *PRR5* and *TOC1* gene expression. Thus, LNKs are important for both transcriptional initiation and elongation, a notion that is also supported by our nascent RNA results. The role of RVE8-LNKs in both transcriptional initiation and elongation might be useful for proper coordination between these two events, favoring transcription efficiency in concert with the production of chromatin marks at the appropriate circadian time. A tight coordination between transcriptional initiation and elongation was shown to be required for the precise regulation of *FLOWERING LOCUS C* expression (Wu et al., 2016), which is also controlled by FACT (Lolas et al., 2010). Our results point to the interesting possibility that LNKs might be important for ensuring a continuous flow from initiation to elongation, avoiding early termination. In the *lnk1 lnk2* double mutant, the initiation and transition to elongation are severely affected, and this explains the severity of the gene expression phenotypes.

Local chromatin organization influences transcription (Smolle and Workman, 2013). H3K4me3 is usually associated with transcriptionally active genes (Gardner et al., 2011). Our results show that H3K4me3 at the *PRR5* and *TOC1* loci is reduced in *lnk1 lnk2* double mutant plants. In yeast (*Saccharomyces cerevisiae*), RNA Pol II activity is required to recruit SET1/COMPASS (Ng et al., 2003), the catalytic subunit of the histone methyl transferase complex that methylates H3K4 (Briggs et al., 2001). In contrast, the sequential order is reversed in mammalian cells, as the presence of H3K4me3 appears to facilitate transcription initiation (Vermeulen et al., 2007). In plants, ATX1 forms a complex with TATA Binding Protein and RNA Pol II to control the formation of the PIC (Ding et al., 2011). Notably, the rhythmic accumulation of H3K4me3 at the promoters of core clock genes parallels the oscillation of clock gene expression. This chromatin signature has been shown to be important for blocking inhibitor binding to clock promoters, thus ensuring proper timing of repression (Malapeira et al., 2012). Our results showing that a chromatin mark is affected in *lnk1 lnk2* double mutant plants is also consistent with previous findings showing that another activating mark, H3 acetylation, is also affected in RVE8-ox and *rve8* mutant plants (Farinas and Mas, 2011). Therefore, the RVE8-LNKs interaction is central for the recruitment of the transcriptional machinery and enables a permissive chromatin environment, favoring clock gene activation and preventing advanced binding of clock repressors.

RNA Pol II transcription requires the coordination of different sets of proteins, including the basal transcription machinery and factors that bind to sequence-specific promoter elements. Here, we have demonstrated that LNKs relay the activating function of the transcription factor RVE8 to the transcriptional machinery. We propose that LNKs act as bridging proteins that function as an important scaffold for the regulation of circadian transcription of core clock genes expressed close to dusk.

METHODS

Plasmid Construction, Plant Material, and Growth Conditions

LNK1 and LNK3 plant overexpression vectors were generated by PCR-mediated amplification of the *LNK1* and *LNK3* coding sequences followed by cloning into the pENTR/D-TOPO vector (Invitrogen). The *LNK1* and *LNK3* coding sequences were subsequently cloned into the plant destination vector pGWB417/517 (Nakagawa et al., 2007a, 2007b) following the manufacturer's recommendations (Invitrogen). RVE8 and domain vectors were generated by cloning RVE8-FL, ΔLCL (nucleotides 1 to 624), and the LCL domain (nucleotides 625 to 885) first into the pENTR/D-TOPO vector and then into the plant destination vector pGWB505 (Nakagawa et al., 2007a, 2007b).

Bacterial expression vectors were generated by cloning the coding sequences of *LNK1*, *SSRP1*, *RNA Pol II CTD*, *RVE8-FL*, *ΔLCL*, and *LCL* into the pENTR/D-TOPO vector. Each coding sequence was subsequently cloned into pDEST565 or pDEST_HIS_MBP (Nallamsetty et al., 2005) vectors using the LR reaction (Invitrogen). For MBP-LNK3, the coding sequence of *LNK3* was amplified by PCR and cloned into the pET_HIS_MBP vector (Bogomolovas et al., 2009) after digestion with *Nco*I and *Xho*I restriction enzymes (Roche) and ligation with T4 DNA ligase (Roche).

Arabidopsis thaliana plants were transformed using *Agrobacterium tumefaciens* (GV2260)-mediated DNA transfer (Clough and Bent, 1998). Seedlings were stratified at 4°C in the dark for 3 d on Murashige and Skoog (MS) agar medium supplemented with 3% sucrose. Plates were transferred to LD (12 h of light/12 h of dark) with 60 to 100 $\mu mol \cdot quanta \cdot m^{-2} \cdot s^{-1}$ cool white fluorescent light at 22°C. The *TOC1pro:LUC* (Perales and Más, 2007), *RVE8-FL-ox* (Farinas and Mas, 2011), *rve8* (SALK_016333C) (Farinas and Mas, 2011), *lnk1 lnk2* (SALK_024353, GK_484F07) (Rugnone et al., 2013), *rve4 rve6 rve8* (Hsu et al., 2013), and *ssrp1-2* (SALK_001283) (Lolas et al., 2010) lines were described elsewhere. Full-length RVE8-ox, ΔLCL-ox, and LCL-ox were transformed into the wild-type background as well as the *rve8* mutant background.

Protein Sequence Alignment and Phylogenetic Analyses

Multiple sequence alignment of the amino acid sequence of the LCL domain was performed using protein sequences from the EnsemblPlants database (http://plants.ensembl.org/index.html). The sequences were subjected to BLAST analysis against the LCL domain of Arabidopsis RVE8. Protein homologs with the closest sequence identity were aligned with ClustalW using the Bioedit program (Bioedit 7.2.5).

Phylogenetic analysis was performed using the maximum likelihood method based on a JTT matrix-based model (Jones et al., 1992). The tree with the highest log likelihood (−923.86) was selected. The initial tree for the heuristic search was obtained by applying Neighbor-Join and BioNJ algorithms to a matrix of pairwise distances estimated using the JTT model and then selecting the topology with superior log likelihood value. The number of bootstrap replicates was 1000. The tree was drawn to scale, with branch lengths measured in the number of substitutions per site (next to the branches). The analysis involved 45 amino acid sequences. All positions containing gaps and missing data were eliminated. There were 56 positions in the final data set. Evolutionary analyses were conducted in MEGA7 (Kumar et al., 2016).

Analyses of Hypocotyl Growth, Flowering Time, and Confocal Imaging

Seeds were stratified on plates with MS agar medium without sucrose for 4 d in the dark at 4°C. Seeds were then exposed to white light (80 $\mu mol \cdot quanta \cdot m^{-2} \cdot s^{-1}$) for 4 h and kept in the dark for 20 h following exposure to constant red light (42 $\mu mol \cdot quanta \cdot m^{-2} \cdot s^{-1}$) for 7 d. Approximately 20 to 25 seedlings were used for hypocotyl length measurements using ImageJ software (National Center for Biotechnology Information [NCBI]). For flowering time assays, seeds were synchronized for 4 d at 4°C and placed on soil. Plants were grown under long-day conditions (16 h of light/8 h of dark) with a light intensity of 80 to 100 $\mu mol \cdot quanta \cdot m^{-2} \cdot s^{-1}$ in walk-in chambers (INKOA). Bolting time and the number of rosette leaves of 10 to 15 plants were counted when the inflorescence stems reached 1 cm high. Two-tailed *t* tests were performed for statistical analyses (*$P < 0.05$, **$P < 0.01$, and ***$P < 0.001$). Two biological replicates were performed with plants grown at different times. Confocal analyses were performed with plants grown on MS agar medium supplemented with 3% sucrose under long-day cycles. Fluorescence signals from hypocotyl and root cells were imaged using an Olympus Fluoview FV1000 confocal microscope with a 515-nm argon laser (excitation, 488 nm; emission, 510 nm).

In Vivo Luminescence Assays

Seven-day-old plants synchronized under LD cycles (12 h of light/12 h of dark) at 22°C were transferred to 96-well plates and resynchronized for an additional 24 h under LD cycles before switching to LL conditions. In vivo luminescence assays were performed as described previously (Takahashi et al., 2015) with an LB960 luminometer (Berthold Technologies) using Microwin software (Mikrotek Laborsysteme). Periods, phases, and amplitudes were estimated using the Fast Fourier Transform-Non-Linear Least Squares suite using the BioDare online tool (www.biodare.ed.ac.uk) (Zielinski et al., 2014). Two-tailed *t* tests were performed for statistical analyses (*$P < 0.05$, **$P < 0.01$, and ***$P < 0.001$). For inhibitor analyses, different concentrations of Flap (1, 5, and 10 μM) and Selic (10, 100, and 500 μM) were vacuum-infiltrated for 5 to 8 min into 7-d-old seedlings before luminescence analyses. Two biological replicates were performed with seedlings grown at different times. Each biological replicate included 8 to 12 seedlings per condition and/or genotype.

Gene Expression Analyses by RT-qPCR

Seedlings were synchronized under LD cycles for 7 d and subsequently transferred to LL for 2 d. Samples were taken every 4 h over the third day under LL. RNA was purified using a Maxwell 16 LEV simplyRNA tissue kit following the manufacturer's recommendations (Promega). Purified RNA was treated with RNase-free Turbo DNase (Ambion), and single-stranded cDNA was synthesized using iScript Reverse Transcription Supermix for RT-qPCR (Bio-Rad) with 1 μg of RNA. qPCR was performed with iTag Universal SYBR Green Supermix (Bio-Rad) or Brilliant III Ultra-Fast SYBR Green qPCR Master Mix (Agilent) with a 96-well CFX96 Touch Real-Time PCR detection system (Bio-Rad). The expression data were normalized to *IPP2* (*ISOPENTENYL PYROPHOSPHATE: DIMETHYL-ALLYL PYROPHSPHATE ISOMERASE*) using the $2^{-\Delta\Delta CT}$ method (Livak and Schmittgen, 2001). For inhibitor analyses, Selic (500 μM) was vacuum-infiltrated for 5 to 8 min into 7-d-old seedlings, and samples were harvested the following day at different circadian times, as indicated. The expression data were normalized to *18S rRNA* using the $2^{-\Delta\Delta CT}$ method (Livak and Schmittgen, 2001). Two biological replicates were performed with seedlings grown and sampled at different times. Two to three technical replicates were performed within the same biological replicate. Primers used in this study are listed in Supplemental Table 1.

Yeast-Two Hybrid Screening

The coding sequence of the LCL domain (nucleotides 625 to 825) was PCR amplified and fused to the C-terminal end of LexA in the pB27 vector. The construct was used as a bait to screen a random-primed cDNA library of

Arabidopsis constructed into the pP6 vector (Hybrigenics Services). Using a mating approach with YHGX13 and L40ΔGal4 strains, ~64 million clones were screened and around 322 His+ colonies were selected on a medium lacking histidine, tryptophan, and leucine. The prey fragments of these positive clones were sequenced and used to search the GenBank database (NCBI) to identify potential interacting proteins with the LCL domain.

Protein Expression, Purification, and in Vitro Pull-Down

Transformed *Escherichia coli* cells (BL21, DE3) were grown until the OD_{600} values reached 0.6 to 0.8. Isopropyl β-D-1-thiogalactopyranosidemediated induction of MBP-LNK3, GST-CTD, and GST-SSRP1 was performed at 28°C for 4 to 6 h. MBP-LNK1, GST-ΔLCL, and GST-LCL were induced at 17°C overnight. Bacteria were lysed by sonication for 2 to 3 min (30 s on, 30 s off, high intensity) using a sonicator (Bioruptor, Diagnode). Recombinant proteins were purified using gravity flow columns with amylose resin for MBP fusion proteins (New England Biolabs) and Glutathione Sepharose 4B for GST-tagged proteins (GE Healthcare). The purified recombinant proteins were concentrated using Amicon centrifugal filters (EMD Millipore).

For in vitro pull-down assays between ΔLCL, LCL, and LNKs, proteins were incubated in pull-down binding buffer (1× PBS, pH 7.4, 0.2% glycerol, 0.6% Triton X-100, and 1 mM β-mercaptoethanol) for 2 h at 4°C with end-over-end rotation. Amylose resin was then added and incubated for another 2 h at 4°C with end-over-end rotation. Beads were washed four to six times with pull-down washing buffer (1× PBS, pH 7.4, 0.6% Triton X-100, and 1 mM β-mercaptoethanol), and protein complexes were released by heating at 95°C for 5 min in 2× SDS loading buffer (100 mM Tris-HCl, pH 6.8, 4% SDS, 0.2% bromophenol blue, 20% glycerol, and 5% β-mercaptoethanol). Protein samples were analyzed by immunoblotting using an anti-MBP antibody (reference sc-809, Santa Cruz Biotechnology) (1:1000 dilution) or a monoclonal anti-GST antibody (reference 8-326; Thermo Fisher Scientific) (1:1000 dilution).

To test the interaction between LNKs and RNA Pol II CTD or SSRP1, proteins were processed as described above with minor modifications. Briefly, proteins were incubated in pull-down binding buffer (20 mM Tris-HCl, pH 7.9, 20% glycerol, 1 mM EDTA, 5 mM $MgCl_2$, 0.1% Nonidet P-40, 1 mM DTT, 0.2 mM PMSF, and 0.1 M NaCl) for 2 h at 4°C with end-over-end rotation. Glutathione Sepharose 4B was then added and incubated for another 2 h at 4°C with end-over-end rotation. Beads were washed four times with pull-down washing buffer (20 mM Tris-HCl, pH 7.9, 20% glycerol, 1 mM EDTA, 5 mM $MgCl_2$, 0.1% Nonidet P-40, 1 mM DTT, 0.2 mM PMSF, and 0.1 M NaCl), and protein complexes were released by heating at 95°C for 5 min in 2× SDS loading buffer (100 mM Tris-HCl, pH 6.8, 4% SDS, 0.2% bromophenol blue, 20% glycerol, and 5% β-mercaptoethanol). Protein samples were analyzed by immunoblotting with an anti-MBP antibody (reference sc-809, Santa Cruz Biotechnology) (1:1000 dilution) or with a monoclonal anti-GST antibody (reference 8-326, Thermo Fisher Scientific) (1:1000 dilution). Two biological replicates were performed per experiment and/or condition.

In Vivo Co-IP Assays in Plants

Analyses of LNKs and LCL interactions were performed with 10-d-old seedlings grown under LD cycles. At least two biological replicates with seedlings grown and sampled at different times were performed. Around 1 g of seedlings was ground in liquid nitrogen and resuspended in 1 mL of co-IP binding buffer (50 mM Tris-HCl, pH 7.5, 150 mM NaCl, 0.4% Nonidet P-40, 1 mM EDTA, 2 mM DTT, 5% glycerol, 1 mM PMSF, 5 μg/mL leupeptin, 1 μg/mL aprotinin, 5 μg/mL antipain, 1 μg/mL pepstatin, 5 μg/mL chymostatin, and 50 μM MG-132). Protein concentration was measured using standard curves with the Bradford method (Bradford, 1976). Supernatants containing equal amounts of total protein were incubated with 25 μL of GFP-trap magnetic beads (Chromotek) for 1 to 2 h at 4°C with end-over-end rotation. Beads were washed with co-IP washing buffer (50 mM Tris-HCl, pH 7.5, 150 mM NaCl, 1 mM EDTA, 2 mM DTT, 1 mM PMSF, 5 μg/mL leupeptin, 1 μg/mL aprotinin, 5 μg/mL antipain, 1 μg/mL pepstatin, 5 μg/mL chymostatin, and 50 μM MG-132). The protein complexes were released from the beads with 50 μL of 2× SDS loading buffer (100 mM Tris-HCl, pH 6.8, 4% SDS, 0.2% bromophenol blue, 20% glycerol, and 5% β-mercaptoethanol) and heating at 95°C for 5 min. The co-IP samples were then analyzed by immunoblot analyses using an anti-GFP antibody (reference A11122, Invitrogen) (1:2500 dilution) and an anti-Myc antibody (reference M4439, Sigma-Aldrich) (1:2500 dilution).

Analyses of the interaction of LNKs with RNA Pol II or SSRP1 were performed following the same protocol described above with slight modifications. Briefly, samples were resuspended in 1 mL of co-IP binding buffer (50 mM Tris-HCl, pH 7.5, 150 mM NaCl, 0.4% Nonidet P-40, 5 mM $MgSO_4$, 2 mM $CaCl_2$, 2 mM DTT, 5% glycerol, 1 mM PMSF, 30 μg/mL leupeptin, 30 μg/mL aprotinin, 30 μg/mL E-64, 7.5 μg/mL antipain, 3 μg/mL pepstatin, 7.5 μg/mL chymostatin, and 50 μM MG-132). Protein concentration was measured using standard curves with the Bradford method (Bradford, 1976). Supernatants containing equal amounts of total protein were treated with DNase I (Promega) or Benzonase (Novagen). Samples were then incubated with 25 μL of Myc-trap agarose beads (Chromotek) for 1 to 2 h at 4°C with end-over-end rotation. Beads were washed with co-IP binding buffer (50 mM Tris-HCl, pH 7.5, 150 mM NaCl, 0.4% Nonidet P-40, 5 mM $MgSO_4$, 2 mM $CaCl_2$, 2 mM DTT, 5% glycerol, 1 mM PMSF, 30 μg/mL leupeptin, 30 μg/mL aprotinin, 30 μg/mL E-64, 7.5 μg/mL antipain, 3 μg/mL pepstatin, 7.5 μg/mL chymostatin, and 50 μM MG-132). Protein complexes were released from the beads using 50 μL of 2× SDS loading buffer (100 mM Tris-HCl, pH 6.8, 4% SDS, 0.2% bromophenol blue, 20% glycerol, and 5% β-mercaptoethanol) and heating at 95°C for 5 min. The co-IP samples were analyzed by immunoblot analysis using a monoclonal anti-Myc antibody (reference M4439, Sigma-Aldrich) (1:2500 dilution), an anti-RNA Pol II CTD repeat YSPTSPS (phospho S2) antibody (reference ab5095, Abcam) (1:1000 dilution), an anti-RNA Pol II CTD repeat YSPTSPS (phospho S5) antibody (reference ab5131, Abcam) (1:1000 dilution), an anti-RNA Pol II antibody (reference at-300, Santa Cruz Biotechnology) (1:1000 dilution), and an anti-SSRP1 antibody (1:1000 dilution) (Duroux et al., 2004). For inhibitor analyses, Selic (300 μM) was vacuum-infiltrated for 8 min into 10-d-old seedlings at ZT3, and samples were harvested at ZT7 the following day. For Ponceau S staining, the membrane was incubated with Ponceau S solution (0.1% Ponceau S and 1% acetic acid) for 5 min with shaking and washed twice by water before imaging.

ChIP and Sequential ChIP Assays

Plants were grown under LD cycles for 10 to 14 d, and samples were collected under LD conditions or the third day under LL at the indicated time points. At least two biological replicates with seedlings grown and sampled at different times were performed. ChIP assays were essentially performed as described previously (Perales and Más, 2007) with some modifications. Briefly, 1 to 2 g of seedlings was fixed in fixation buffer (10 mM Tris-HCl, pH 8.0, 0.4 M sucrose, 1 mM EDTA, 1 mM PMSF, 0.25% Triton X-100, and 1% formaldehyde) for 10 to 15 min under a vacuum. The fixation was stopped by adding glycine to a final concentration of 0.125 M and vacuum for 10 min. Seedlings were washed twice with 50 mL of cold water, frozen in liquid nitrogen, and stored at −80°C. Samples were ground in liquid nitrogen to a fine powder and resuspended in extraction buffer I (10 mM Tris-HCl, pH 8.0, 0.4 M sucrose, 5 mM EDTA, 5 mM β-mercaptoethanol, 1 mM PMSF, 5 μg/mL leupeptin, 1 μg/mL aprotinin, 1 μg/mL E-64, 5 μg/mL antipain, 1 μg/mL pepstatin, 5 μg/mL chymostatin, and 50 μM MG-132). Following filtration with Miracloth (EMD Millipore), the cells were centrifuged at 1000*g* for 20 min and washed with extraction buffer II (10 mM Tris-HCl, pH 8.0, 0.25 M sucrose, 10 mM $MgCl_2$, 1% Triton X-100, 5 mM EDTA, 5 mM

β-mercaptoethanol, 1 mM PMSF, 5 μg/mL leupeptin, 1 μg/mL aprotinin, 1 μg/mL E-64, 5 μg/mL antipain, 1 μg/mL pepstatin, 5 μg/mL chymostatin, and 50 μM MG-132) to purify nuclei. The nuclei were then resuspended in 1 mL of nuclei lysis buffer (10 mM Tris-HCl, pH 8.0, 10 mM EDTA, 1% SDS, 1 mM PMSF, 5 μg/mL leupeptin, 1 μg/mL aprotinin, 1 μg/mL E-64, 5 μg/mL antipain, 1 μg/mL pepstatin, 5 μg/mL chymostatin, and 50 μM MG-132) and sonicated 4 min (30 s on, 30 s off, low intensity) with a sonicator (Bioruptor, Diagnode). Nuclear debris was removed by centrifugation at maximum speed. Approximately 20 to 25 μg of chromatin was then diluted with 1 mL of ChIP dilution buffer (15 mM Tris-HCl, pH 8.0, 167 mM NaCl, 1 mM EDTA, 1.1% Triton X-100, 1 mM PMSF, 5 μg/mL leupeptin, 1 μg/mL aprotinin, 5 μg/mL antipain, 1 μg/mL pepstatin, 5 μg/mL chymostatin, and 50 μM MG-132) and incubated with the corresponding antibody overnight at 4°C. Protein-DNA complexes were collected by incubation with 50 μL of equilibrated Protein G beads (Dynabeads, Invitrogen) for 2 to 3 h. The beads were sequentially washed with low-salt buffer (20 mM Tris-HCl, pH 8.0, 150 mM NaCl, 1% Triton X-100, 2 mM EDTA, 0.1% SDS, 1 mM PMSF, 5 μg/mL leupeptin, 1 μg/mL aprotinin, 1 μg/mL E-64, 5 μg/mL antipain, 1 μg/mL pepstatin, 5 μg/mL chymostatin, and 50 μM MG-132), high-salt buffer (20 mM Tris-HCl, pH 8.0, 500 mM NaCl, 1% Triton X-100, 2 mM EDTA, 0.1% SDS, 1 mM PMSF, 5 μg/mL leupeptin, 1 μg/mL aprotinin, 1 μg/mL E-64, 5 μg/mL antipain, 1 μg/mL pepstatin, 5 μg/mL chymostatin, and 50 μM MG-132), LiCl buffer (10 mM Tris-HCl, pH 8.0, 1 mM EDTA, 250 mM LiCl, 1% Nonidet P-40, 1% sodium deoxycholate, 1 mM PMSF, 5 μg/mL leupeptin, 1 μg/mL aprotinin, 1 μg/mL E-64, 5 μg/mL antipain, 1 μg/mL pepstatin, 5 μg/mL chymostatin, and 50 μM MG-132), and TE buffer (10 mM Tris-HCl, pH 8.0, and 1 mM EDTA). Protein-DNA complexes were released by incubation with 300 μL of ChIP elution buffer for 1 h at 65°C. Reverse cross-linking was performed by adding 0.2 M NaCl and incubating at 65°C overnight. DNA was purified using a Gel Extraction Kit (Qiagen) following the manufacturer's recommendation. qPCR was performed with iTag Universal SYBR Green Supermix (Bio-Rad) or Brilliant III Ultra-Fast SYBR Green qPCR Master Mix (Agilent) using a 96-well CFX96 Touch Real-Time PCR detection system (Bio-Rad). For inhibitor analyses, Flap (10 μM) or Selic (300 μM) was vacuum-infiltrated for 8 min into 12-d-old seedlings at ZT3, and samples were harvested at ZT7 the following day. To take into account differences in the immunoprecipitation efficiency in the different samples, *ACT7* was used as a positive control in ChIP assays of the basal transcriptional machinery. For ChIP analyses with LNKs or RVE8 domains, it is obviously not possible to use *ACT7* as a positive control. A two-tailed *t* test was performed for statistical analysis (*$P < 0.05$, **$P < 0.01$, and ***$P < 0.001$).

Sequential ChIP assays (Xie and Grotewold, 2008) were performed following the same ChIP procedure described above but including 2× washes with low-salt buffer (20 mM Tris-HCl, pH 8.0, 150 mM NaCl, 1% Triton X-100, 0.1% SDS, 2 mM EDTA, 1 mM PMSF, 5 μg/mL leupeptin, 1 μg/mL aprotinin, 1 μg/mL E-64, 5 μg/mL antipain, 1 μg/mL pepstatin, 5 μg/mL chymostatin, and 50 μM MG-132) and 2× washes with TE buffer (10 mM Tris-HCl, pH 8.0, and 1 mM EDTA) after the first round of immunoprecipitation with the anti-MYC antibody (reference M4439, Sigma-Aldrich) (1:500 dilution). Complexes were eluted with 15 mM DTT and incubated at 37°C for 30 min. Chromatin was then diluted in Sequential ChIP buffer (15 mM Tris-HCl, pH 8.0, 150 mM NaCl, 1 mM EDTA, 1 mM PMSF, 5 μg/mL leupeptin, 1 μg/mL aprotinin, 5 μg/mL antipain, 1 μg/mL pepstatin, 5 μg/mL chymostatin, and 50 μm MG132) and concentrated using Amicon centrifugal filters (EMD Millipore). Samples were then incubated overnight at 4°C either with an anti-Myc antibody (reference M4439, Sigma-Aldrich) (1:500 dilution) or with an anti-SSRP1 antibody (Duroux et al., 2004) (1:200 dilution). Complexes were washed, eluted, purified, and amplified as described above.

Nascent RNAs

Nascent RNA analyses were performed as described previously (Hetzel et al., 2016) with minor modifications. Briefly, seedlings were grown in MS medium supplemented with 3% sucrose for 5 d under LD cycles at 22°C. Plates were then moved to LL conditions, and ~20-g samples were collected at the indicated time points on the third day under LL. At least two biological replicates with seedlings grown and sampled at different times were performed. Samples were homogenized with an Ultra Turrax T-25 homogenizer in 100 mL of ice-cold grinding buffer (300 mM sucrose, 20 mM Tris, pH 8.0, 5 mM $MgCl_2$, 5 mM KCl, 0.2% [v/v] Triton X-100, 5 mM β-mercaptoethanol, and 35% [v/v] glycerol) at 4°C. Samples were then filtered through Miracloth (EMD Millipore) before being passed through a 60-μm cell strainer into 50-mL Falcon tubes. Tubes were centrifuged at 5000*g* for 10 min at 4°C. Pellets were then washed twice by homogenization with 30 mL of cold grinding buffer using a microstreaker. Pellets were resuspended in 2 mL of freezing buffer (50 mM Tris, pH 8.0, 5 mM $MgCl_2$, 20% [v/v] glycerol, and 5 mM β-mercaptoethanol), and nuclei were counted under a light microscope using a Neubauer chamber. Nuclei were then divided into aliquots in 1.5-mL tubes and frozen in liquid N_2. Nuclear run-on of ~5 to 6 × 10^6 nuclei was performed by adding 200 μL of 3× nuclear run-on reaction buffer (15 mM Tris-HCl, pH 8.0, 450 mM KCl, 7.5 mM $MgCl_2$, 1.5% [v/v] 20% sarkosyl, 1.5 mM DTT, 0.2 units/μL SUPERase-in [Fisher Scientific], 375 μM ATP, 375 μM GTP, 60 nM CTP, and 375 μM BrUTP [Sigma-Aldrich]). After 5 min of incubation at room temperature, run-on was stopped by adding 140 μL of DNase Mix (15 μL of 10× RQ1 DNase I buffer, 50 μL of nuclease-free deionized water, and 5 μL of RQ1 DNase [Promega]) for 15 min at room temperature, followed by the addition of 160 μL of STOP Mix (20 mM EDTA, 200 mM NaCl, 1% [v/v] SDS, and 0.3 mg/mL glycogen) plus 20 μL of 2.5 mg/mL proteinase K and incubation for 30 min at 37°C. Nuclei were centrifuged for 10 min at 1000*g* at 4°C, and RNA was extracted using a TRIzol-based protocol in which 250 μL of high-salt buffer (0.8 M sodium citrate [$NaH_2(C_3H_5O(COO)_3)$] and 1.2 M NaCl) and 1 μL of RNase-free glycogen were added for isopropanol precipitation. Prior to BrUTP precipitation, BrdU antibody beads (sc-32323 AC; Santa Cruz Biotechnology) were washed twice with ice-cold GRO binding buffer (0.25× saline-sodium-phosphate-EDTA buffer, 0.05% [v/v] Tween, 37.5 mM NaCl, and 1 mM EDTA). Approximately 50 μL of each RNA sample was diluted with 450 μL of cold GRO binding buffer and incubated with 40 μL of equilibrated BrdU antibody beads. The reaction was incubated under slow rotation for 1.5 h at 4°C. Beads were spun down for 20 min at 1000*g* at 4°C. Beads were then resuspended in 200 μL of cold grinding buffer and transferred to a Millipore MC column (UFC30HVNB EMD Millipore). After a spin down for 1 min at 1000*g*, beads were washed twice with 500 μL of cold grinding buffer for 5 min under fast rotation at 4°C. Columns were then moved to fresh 1.5-mL tubes, and RNA was eluted with 200 μL of TRIzol LS under gentle shaking for 5 min at room temperature. After a second TRIzol elution, 100 μL of nuclease-free deionized water was added to the column and eluted. RNA was extracted using a TRIzol-based protocol following the manufacturer's recommendations. cDNA synthesis was performed as described previously (Roberts et al., 2015). A High-Capacity cDNA Reverse Transcription Kit (Thermo Fisher Scientific) was used for reverse transcriptase-mediated PCR. RT-qPCR analyses were performed in a CFX96 Touch Real-Time PCR detection system using Brilliant III Ultra-Fast SYBR Green qPCR Master Mix (Agilent Technologies). The primers used for nascent RNA detection span exon-intron boundaries in order to exclude the amplification of mature mRNA, which was also verified by the use of primers amplifying exon-exon boundaries. Nascent RNA primers for *ACT7* and *UBQ5* were used as controls. The expression data were analyzed using the $2^{-\Delta\Delta CT}$ method (Livak and Schmittgen, 2001). The primers used are listed in Supplemental Table 1.

Accession Numbers

Sequence data in this study can be found in the Arabidopsis Genome Initiative under the following accession numbers: *RVE8* (AT3G09600), *LNK1* (AT5G64170), *LNK2* (AT3G54500), *LNK3* (AT3G12320), *LNK4*

(AT5G06980), *SSRP1* (AT3G28730), *SPT16* (AT4G10710), *RNA Pol II* (AT4G35800), *TOC1* (AT5G61380), *PRR5* (AT5G24470), *ACT7* (AT5G09810), *UBQ5* (AT3G62250), *PPR* (AT5G55840), *IPP2* (AT3G02780), and *TA3* (AT1G37110).

Supplemental Data

Supplemental Figure 1. Characterization of ΔLCL-ox.

Supplemental Figure 2. Multiple Sequence Alignment of the LCL Domain Amino Acid Sequence in Plants.

Supplemental Figure 3. Phylogenetic Analysis of the Closest Homologs to RVE8.

Supplemental Figure 4. Characterization of LCL-ox.

Supplemental Figure 5. Direct Interaction of LNKs with the LCL Domain of RVE8 and Total RNA Pol II Accumulation at the *PRR5* and *TOC1* Loci.

Supplemental Figure 6. In Vitro Interaction of LNK1 with RNA Pol II and Binding of LNK1 and RVE8 to the *PRR5* and *TOC1* Loci.

Supplemental Figure 7. LNKs and SSRP1 Are Important for RNA Pol II Recruitment at Core Clock Loci.

Supplemental Figure 8. Analyses of RNA Pol II S5P and S2P Inhibition.

Supplemental Figure 9. Role of LNKs in the Regulation of *PRR5* and *TOC1* Transcript Synthesis.

Supplemental Table 1. Primers Used in This Study.

ACKNOWLEDGMENTS

We thank Sascha H.C. Duttke (University of California, San Diego) and Jonathan Hetzel (Salk Institute, La Jolla) for insightful details about the nascent RNAs protocol. We thank G.A. Pizzio for insightful comments on the manuscript. We also thank Tsuyoshi Nakagawa (Shimane University) for providing the Gateway binary vectors and Stacey Harmer for the *rve4/6/8* mutant. The K.D.G. laboratory is funded by the European Commission Marie Curie Research Training Network (ChIP-ET) and by the German Research Foundation through Grant Gr1159/14-1. The P.M. laboratory is funded by the Spanish Ministry of Economy and Competitiveness, from the European Regional Development Fund, from the Generalitat de Catalunya (AGAUR), from the Global Research Network of the National Research Foundation of Korea, from the European Commission Marie Curie Research Training Network (ChIP-ET), and by the CERCA Programme/Generalitat de Catalunya. We acknowledge financial support from the Spanish Ministry of Economy and Competitiveness through the "Severo Ochoa Programme for Centres of Excellence in R&D" 2016-2019 (SEV-2015-0533). Y.M. was supported by a PhD fellowship from the China Scholarship Council and S.G. by a Formación de Personal Investigador fellowship (Ministerio de Economía y Competitividad).

AUTHOR CONTRIBUTIONS

Y.M. and S.G. performed the experiments. K.D.G. provided reagents and constructive comments on the manuscript. P.M. designed the experiments, analyzed the data, and wrote the manuscript. All authors read, revised, and approved the research article.

Received February 27, 2018; revised April 2, 2018; accepted April 2, 2018; published April 4, 2018.

REFERENCES

Allison, L.A., Wong, J.K., Fitzpatrick, V.D., Moyle, M., and Ingles, C.J. (1988). The C-terminal domain of the largest subunit of RNA polymerase II of *Saccharomyces cerevisiae*, *Drosophila melanogaster*, and mammals: a conserved structure with an essential function. Mol. Cell. Biol. **8:** 321–329.

Antosz, W., et al. (2017). The composition of the Arabidopsis RNA polymerase II transcript elongation complex reveals the interplay between elongation and mRNA processing factors. Plant Cell **29:** 854–870.

Birse, C.E., Minvielle-Sebastia, L., Lee, B.A., Keller, W., and Proudfoot, N.J. (1998). Coupling termination of transcription to messenger RNA maturation in yeast. Science **280:** 298–301.

Bogomolovas, J., Simon, B., Sattler, M., and Stier, G. (2009). Screening of fusion partners for high yield expression and purification of bioactive viscotoxins. Protein Expr. Purif. **64:** 16–23.

Bordage, S., Sullivan, S., Laird, J., Millar, A.J., and Nimmo, H.G. (2016). Organ specificity in the plant circadian system is explained by different light inputs to the shoot and root clocks. New Phytol. **212:** 136–149.

Bradford, M.M. (1976). A rapid and sensitive method for the quantitation of microgram quantities of protein utilizing the principle of protein-dye binding. Anal. Biochem. **72:** 248–254.

Briggs, S.D., Bryk, M., Strahl, B.D., Cheung, W.L., Davie, J.K., Dent, S.Y.R., Winston, F., and Allis, C.D. (2001). Histone H3 lysine 4 methylation is mediated by Set1 and required for cell growth and rDNA silencing in *Saccharomyces cerevisiae*. Genes Dev. **15:** 3286–3295.

Buratowski, S. (2009). Progression through the RNA polymerase II CTD cycle. Mol. Cell **36:** 541–546.

Carré, I.A., and Kim, J.-Y. (2002). MYB transcription factors in the Arabidopsis circadian clock. J. Exp. Bot. **53:** 1551–1557.

Clough, S.J., and Bent, A.F. (1998). Floral dip: a simplified method for Agrobacterium-mediated transformation of *Arabidopsis thaliana*. Plant J. **16:** 735–743.

Ding, Y., Avramova, Z., and Fromm, M. (2011). Two distinct roles of ARABIDOPSIS HOMOLOG OF TRITHORAX1 (ATX1) at promoters and within transcribed regions of ATX1-regulated genes. Plant Cell **23:** 350–363.

Ding, Y., Ndamukong, I., Xu, Z., Lapko, H., Fromm, M., and Avramova, Z. (2012). ATX1-generated H3K4me3 is required for efficient elongation of transcription, not initiation, at ATX1-regulated genes. PLoS Genet. **8:** e1003111.

Du, H., Zhang, L., Liu, L., Tang, X.F., Yang, W.J., Wu, Y.M., Huang, Y.B., and Tang, Y.X. (2009). Biochemical and molecular characterization of plant MYB transcription factor family. Biochemistry (Mosc.) **74:** 1–11.

Dubos, C., Stracke, R., Grotewold, E., Weisshaar, B., Martin, C., and Lepiniec, L. (2010). MYB transcription factors in Arabidopsis. Trends Plant Sci. **15:** 573–581.

Duroux, M., Houben, A., Růzicka, K., Friml, J., and Grasser, K.D. (2004). The chromatin remodelling complex FACT associates with actively transcribed regions of the *Arabidopsis* genome. Plant J. **40:** 660–671.

Endo, M., Shimizu, H., Nohales, M.A., Araki, T., and Kay, S.A. (2014). Tissue-specific clocks in Arabidopsis show asymmetric coupling. Nature **515:** 419–422.

Farinas, B., and Mas, P. (2011). Functional implication of the MYB transcription factor RVE8/LCL5 in the circadian control of histone acetylation. Plant J. **66:** 318–329.

Gardner, K.E., Allis, C.D., and Strahl, B.D. (2011). Operating on chromatin, a colorful language where context matters. J. Mol. Biol. **409:** 36–46.

Gray, J.A., Shalit-Kaneh, A., Chu, D.N., Hsu, P.Y., and Harmer, S.L. (2017). The REVEILLE clock genes inhibit growth of juvenile and adult plants by control of cell size. Plant Physiol. **173:** 2308–2322.

Greenham, K., and McClung, C.R. (2015). Integrating circadian dynamics with physiological processes in plants. Nat. Rev. Genet. **16:** 598–610.

Hajheidari, M., Koncz, C., and Eick, D. (2013). Emerging roles for RNA polymerase II CTD in Arabidopsis. Trends Plant Sci. **18:** 633–643.

Hetzel, J., Duttke, S.H., Benner, C., and Chory, J. (2016). Nascent RNA sequencing reveals distinct features in plant transcription. Proc. Natl. Acad. Sci. USA **113:** 12316–12321.

Hsu, P.Y., Devisetty, U.K., and Harmer, S.L. (2013). Accurate timekeeping is controlled by a cycling activator in Arabidopsis. eLife **2:** e00473.

Hyun, Y., Richter, R., Vincent, C., Martinez-Gallegos, R., Porri, A., and Coupland, G. (2016). Multi-layered regulation of SPL15 and cooperation with SOC1 integrate endogenous flowering pathways at the Arabidopsis shoot meristem. Dev. Cell **37:** 254–266.

James, A.B., Monreal, J.A., Nimmo, G.A., Kelly, C.L., Herzyk, P., Jenkins, G.I., and Nimmo, H.G. (2008). The circadian clock in Arabidopsis roots is a simplified slave version of the clock in shoots. Science **322:** 1832–1835.

Jin, H., and Martin, C. (1999). Multifunctionality and diversity within the plant MYB-gene family. Plant Mol. Biol. **41:** 577–585.

Jones, D.T., Taylor, W.R., and Thornton, J.M. (1992). The rapid generation of mutation data matrices from protein sequences. Comput. Appl. Biosci. **8:** 275–282.

Jonkers, I., and Lis, J.T. (2015). Getting up to speed with transcription elongation by RNA polymerase II. Nat. Rev. Mol. Cell Biol. **16:** 167–177.

Komarnitsky, P., Cho, E.-J., and Buratowski, S. (2000). Different phosphorylated forms of RNA polymerase II and associated mRNA processing factors during transcription. Genes Dev. **14:** 2452–2460.

Kumar, S., Stecher, G., and Tamura, K. (2016). MEGA7: Molecular Evolutionary Genetics Analysis version 7.0 for bigger datasets. Mol. Biol. Evol. **33:** 1870–1874.

Lee, Y.C., Park, J.M., Min, S., Han, S.J., and Kim, Y.-J. (1999). An activator binding module of yeast RNA polymerase II holoenzyme. Mol. Cell. Biol. **19:** 2967–2976.

Livak, K.J., and Schmittgen, T.D. (2001). Analysis of relative gene expression data using real-time quantitative PCR and the 2(-Δ Δ C (T)) method. Methods **25:** 402–408.

Lolas, I.B., Himanen, K., Gronlund, J.T., Lynggaard, C., Houben, A., Melzer, M., Van Lijsebettens, M., and Grasser, K.D. (2010). The transcript elongation factor FACT affects Arabidopsis vegetative and reproductive development and genetically interacts with HUB1/2. Plant J. **61:** 686–697.

Malapeira, J., Khaitova, L.C., and Mas, P. (2012). Ordered changes in histone modifications at the core of the Arabidopsis circadian clock. Proc. Natl. Acad. Sci. USA **109:** 21540–21545.

Margaritis, T., and Holstege, F.C.P. (2008). Poised RNA polymerase II gives pause for thought. Cell **133:** 581–584.

Mason, P.B., and Struhl, K. (2005). Distinction and relationship between elongation rate and processivity of RNA polymerase II in vivo. Mol. Cell **17:** 831–840.

McCracken, S., Fong, N., Yankulov, K., Ballantyne, S., Pan, G., Greenblatt, J., Patterson, S.D., Wickens, M., and Bentley, D.L. (1997). The C-terminal domain of RNA polymerase II couples mRNA processing to transcription. Nature **385:** 357–361.

Menet, J.S., Rodriguez, J., Abruzzi, K.C., and Rosbash, M. (2012). Nascent-Seq reveals novel features of mouse circadian transcriptional regulation. eLife **1:** e00011.

Mizuno, T., Takeuchi, A., Nomoto, Y., Nakamichi, N., and Yamashino, T. (2014). The *LNK1* night light-inducible and clock-regulated gene is induced also in response to warm-night through the circadian clock nighttime repressor in *Arabidopsis thaliana*. Plant Signal. Behav. **9:** e28505.

Näär, A.M., Lemon, B.D., and Tjian, R. (2001). Transcriptional coactivator complexes. Annu. Rev. Biochem. **70:** 475–501.

Nakagawa, T., et al. (2007b). Improved Gateway binary vectors: high-performance vectors for creation of fusion constructs in transgenic analysis of plants. Biosci. Biotechnol. Biochem. **71:** 2095–2100.

Nakagawa, T., Kurose, T., Hino, T., Tanaka, K., Kawamukai, M., Niwa, Y., Toyooka, K., Matsuoka, K., Jinbo, T., and Kimura, T. (2007a). Development of series of Gateway binary vectors, pGWBs, for realizing efficient construction of fusion genes for plant transformation. J. Biosci. Bioeng. **104:** 34–41.

Nallamsetty, S., Austin, B.P., Penrose, K.J., and Waugh, D.S. (2005). Gateway vectors for the production of combinatorially-tagged His6-MBP fusion proteins in the cytoplasm and periplasm of *Escherichia coli*. Protein Sci. **14:** 2964–2971.

Nawrath, C., Schell, J., and Koncz, C. (1990). Homologous domains of the largest subunit of eucaryotic RNA polymerase II are conserved in plants. Mol. Gen. Genet. **223:** 65–75.

Ng, H.H., Robert, F., Young, R.A., and Struhl, K. (2003). Targeted recruitment of Set1 histone methylase by elongating Pol II provides a localized mark and memory of recent transcriptional activity. Mol. Cell **11:** 709–719.

Orphanides, G., LeRoy, G., Chang, C.-H., Luse, D.S., and Reinberg, D. (1998). FACT, a factor that facilitates transcript elongation through nucleosomes. Cell **92:** 105–116.

Perales, M., and Más, P. (2007). A functional link between rhythmic changes in chromatin structure and the Arabidopsis biological clock. Plant Cell **19:** 2111–2123.

Pérez-García, P., Ma, Y., Yanovsky, M.J., and Mas, P. (2015). Time-dependent sequestration of RVE8 by LNK proteins shapes the diurnal oscillation of anthocyanin biosynthesis. Proc. Natl. Acad. Sci. USA **112:** 5249–5253.

Preker, P., Nielsen, J., Kammler, S., Lykke-Andersen, S., Christensen, M.S., Mapendano, C.K., Schierup, M.H., and Jensen, T.H. (2008). RNA exosome depletion reveals transcription upstream of active human promoters. Science **322:** 1851–1854.

Rawat, R., Takahashi, N., Hsu, P.Y., Jones, M.A., Schwartz, J., Salemi, M.R., Phinney, B.S., and Harmer, S.L. (2011). REVEILLE8 and PSEUDO-REPONSE REGULATOR5 form a negative feedback loop within the Arabidopsis circadian clock. PLoS Genet. **7:** e1001350.

Roberts, T.C., Hart, J.R., Kaikkonen, M.U., Weinberg, M.S., Vogt, P.K., and Morris, K.V. (2015). Quantification of nascent transcription by bromouridine immunocapture nuclear run-on RT-qPCR. Nat. Protoc. **10:** 1198–1211.

Rodriguez, J., Tang, C.H., Khodor, Y.L., Vodala, S., Menet, J.S., and Rosbash, M. (2013). Nascent-Seq analysis of Drosophila cycling gene expression. Proc. Natl. Acad. Sci. USA **110:** E275–E284.

Rugnone, M.L., Faigón Soverna, A., Sanchez, S.E., Schlaen, R.G., Hernando, C.E., Seymour, D.K., Mancini, E., Chernomoretz, A., Weigel, D., Más, P., and Yanovsky, M.J. (2013). LNK genes integrate light and clock signaling networks at the core of the Arabidopsis oscillator. Proc. Natl. Acad. Sci. USA **110:** 12120–12125.

Shukla, A., Chaurasia, P., and Bhaumik, S.R. (2009). Histone methylation and ubiquitination with their cross-talk and roles in gene expression and stability. Cell. Mol. Life Sci. **66:** 1419–1433.

Smolle, M., and Workman, J.L. (2013). Transcription-associated histone modifications and cryptic transcription. Biochim. Biophys. Acta **1829:** 84–97.

Takahashi, N., Hirata, Y., Aihara, K., and Mas, P. (2015). A hierarchical multi-oscillator network orchestrates the Arabidopsis circadian system. Cell **163:** 148–159.

Thain, S.C., Murtas, G., Lynn, J.R., McGrath, R.B., and Millar, A.J. (2002). The circadian clock that controls gene expression in Arabidopsis is tissue specific. Plant Physiol. **130:** 102–110.

Van Lijsebettens, M., and Grasser, K.D. (2014). Transcript elongation factors: shaping transcriptomes after transcript initiation. Trends Plant Sci. **19:** 717–726.

Vermeulen, M., Mulder, K.W., Denissov, S., Pijnappel, W.W.M.P., van Schaik, F.M.A., Varier, R.A., Baltissen, M.P.A., Stunnenberg, H.G., Mann, M., and Timmers, H.T.M. (2007). Selective anchoring of TFIID to nucleosomes by trimethylation of histone H3 lysine 4. Cell **131:** 58–69.

Wenden, B., Toner, D.L.K., Hodge, S.K., Grima, R., and Millar, A.J. (2012). Spontaneous spatiotemporal waves of gene expression from biological clocks in the leaf. Proc. Natl. Acad. Sci. USA **109:** 6757–6762.

Wu, Z., Ietswaart, R., Liu, F., Yang, H., Howard, M., and Dean, C. (2016). Quantitative regulation of FLC via coordinated transcriptional initiation and elongation. Proc. Natl. Acad. Sci. USA **113:** 218–223.

Xie, Q., et al. (2014). LNK1 and LNK2 are transcriptional coactivators in the Arabidopsis circadian oscillator. Plant Cell **26:** 2843–2857.

Xie, Z., and Grotewold, E. (2008). Serial ChIP as a tool to investigate the co-localization or exclusion of proteins on plant genes. Plant Methods **4:** 25.

Xin, H., Takahata, S., Blanksma, M., McCullough, L., Stillman, D.J., and Formosa, T. (2009). yFACT induces global accessibility of nucleosomal DNA without H2A-H2B displacement. Mol. Cell **35:** 365–376.

Xing, H., Wang, P., Cui, X., Zhang, C., Wang, L., Liu, X., Yuan, L., Li, Y., Xie, Q., and Xu, X. (2015). LNK1 and LNK2 recruitment to the evening element require morning expressed circadian related MYB-like transcription factors. Plant Signal. Behav. **10:** e1010888.

Yakir, E., Hassidim, M., Melamed-Book, N., Hilman, D., Kron, I., and Green, R.M. (2011). Cell autonomous and cell-type specific circadian rhythms in Arabidopsis. Plant J. **68:** 520–531.

Zhang, E.E., and Kay, S.A. (2010). Clocks not winding down: unravelling circadian networks. Nat. Rev. Mol. Cell Biol. **11:** 764–776.

Zielinski, T., Moore, A.M., Troup, E., Halliday, K.J., and Millar, A.J. (2014). Strengths and limitations of period estimation methods for circadian data. PLoS One **9:** e96462.